A 3D FDTD code implemented in MATLAB

Contents

Section I. Yee grid and finite differences

1. Yee grid

A cubic Yee unit cell (uniform cell size Δ in all directions) is shown in Fig. 1. It has the following features [1]:

1. The electric field is defined at the edge centers of a cube;
2. The magnetic field is defined at the face centers of a cube;
3. The electric permittivity/conductivity is defined at the cube center(s);
4. The magnetic permeability/magnetic loss is defined at the cube nodes (corners).

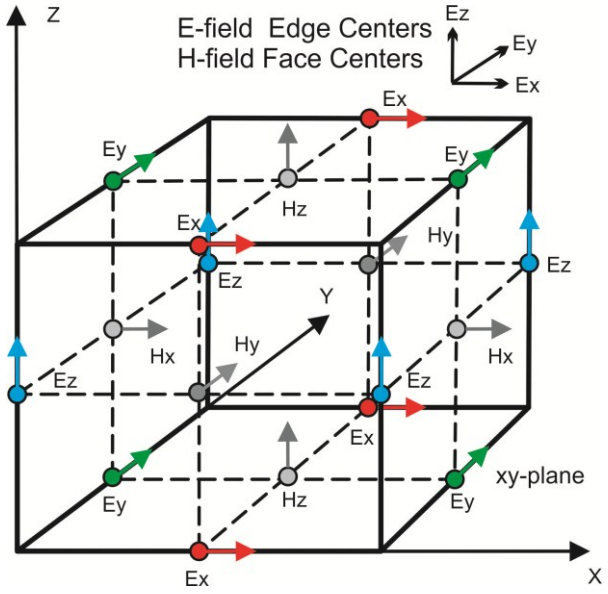

Fig. 1. Yee unit cell.

Therefore, four interleaving indexing systems (i,j,k) in space may be introduced and used simultaneously:

i. the system based on cube edge centers (for the electric field);
ii. the system based on cube face centers (for the magnetic field);
iii. the system based on cube centers (for electric permittivity/conductivity values);

iv. the system based on cube nodes (for magnetic permeability/magnetic loss values);

The interleaving feature of those systems is mathematically described by half-integer indexes. For example, when the indexing system for the magnetic field is used, the nodal magnetic field $H_y\big|_{i,j,k}$ is located exactly halfway between electric field nodes $E_z\big|_{i-1/2,j,k}$ and $E_z\big|_{i+1/2,j,k}$ in Fig. 1. Similarly, when the indexing system for the electric field is used, the nodal electric field $E_z\big|_{i,j,k}$ is located exactly halfway between magnetic field nodes $H_y\big|_{i-1/2,j,k}$ and $H_y\big|_{i+1/2,j,k}$ in Fig. 1, except for the boundary nodes.

2. Maxwell's equations in three dimensions

2.1. Lossless space with no sources

Consider an arbitrary (inhomogeneous) medium with electric permittivity ε having the units of F/m and with magnetic permeability μ having the units of H/m. In free lossless space (space without sources), Maxwell's equations for the electric field (or the electric field intensity) $\vec{E}$ [V/m] and for the magnetic field (or the magnetic field intensity) $\vec{H}$ [A/m] in time domain have the form

Maxwell's $\nabla\times\vec{H}$ equation $$\varepsilon\frac{\partial\vec{E}}{\partial t}=\nabla\times\vec{H} \qquad (1a)$$

Faraday's law $$\mu\frac{\partial\vec{H}}{\partial t}=-\nabla\times\vec{E} \qquad (1b)$$

Gauss' law for electric field (no electric charges) $$\nabla\cdot\varepsilon\vec{E}=0 \qquad (1c)$$

Gauss' law for magnetic field (no magnetic charges) $$\nabla\cdot\mu\vec{H}=0 \qquad (1d)$$

2.2. Driving sources and lossy space

The *driving sources* for the electromagnetic fields are given by (generally volumetric) *electric current density* $\vec{J}_s$ of free charges with the units of A/m^2, and by volumetric *free charge density* ρ_s with the units of C/m^3. The free charges are free electrons in a metal or free electrons and/or holes in a semiconductor. Instead of volumetric currents one may consider surface currents (a blade metal dipole) or line current (an infinitesimally thin cylindrical dipole/wire).

The driving sources may be also given by a (volumetric) *magnetic current density* $\vec{J}_{ms}$ with the units of V/m^2 and by volumetric *magnetic charge density* ρ_{ms}. The magnetic current density may be associated with an external impressed voltage. However, no magnetic charge has been found to exist in nature. Still, in practice it is often convenient to use the concept of magnetic currents (and fictitious magnetic charges).

The *electric conduction current* is always present in a lossy medium in the form $\vec{J} = \sigma\vec{E}$ where σ is the electric conductivity with the units of S/m. So does an equivalent magnetic conduction current describing the magnetic loss mechanism, $\vec{J}_m = \bar{\rho}\vec{H}$ where $\bar{\rho}$ is the equivalent magnetic resistivity with the units of Ω/m.

In a lossy space with driving sources, Maxwell's equations for the electric field (or the electric field intensity) $\vec{E}$ [V/m] and for the magnetic field (or the magnetic field intensity) $\vec{H}$ [A/m] in time domain have the form

Ampere's law modified by displacement currents $$\varepsilon\frac{\partial\vec{E}}{\partial t} = \nabla\times\vec{H} - \vec{J} - \vec{J}_S \qquad (2a)$$

Faraday's law $$\mu\frac{\partial\vec{H}}{\partial t} = -\nabla\times\vec{E} - \vec{J}_m - \vec{J}_{ms} \qquad (2b)$$

Gauss' law for electric field $$\nabla\cdot\varepsilon\vec{E} = \rho_s \qquad (2c)$$

Gauss' law for magnetic field (no magnetic charges) $$\nabla\cdot\mu\vec{H} = \rho_{ms} \qquad (2d)$$

Continuity equation for the impressed electric current $$\frac{\partial\rho_s}{\partial t} + \nabla\cdot\vec{J}_s = 0 \qquad (2e)$$

Continuity equation for the impressed magnetic current $$\frac{\partial\rho_{ms}}{\partial t} + \nabla\cdot\vec{J}_{ms} = 0 \qquad (2e)$$

A comprehensive theory of engineering electromagnetics may be found elsewhere [2],[3].

2.3. Divergence-free fields

It is critical for FDTD to have the divergence-free electric and magnetic fields, with the distributed electric and magnetic charges being equal to zero, even for the point sources. This may be achieved using the loops of currents:

(i) the closed loop of electric current to model the magnetic dipole (a small coil or loop antenna) and;
(ii) the closed loop of magnetic current to model the electric dipole (a small current element). The loops of current (electric or magnetic) do not possess the (net) charge. Other methods include dumping charges into lumped resistors, etc.

3. Maxwell's equations on Yee grid

3.1. Half-grid formulation

Applying the central differences to all derivatives in Eqs. (1) and denoting the temporal grid by a superscript *n*, one arrives at the following finite-difference update equations [4]:

Determine magnetic field at half temporal grid using the past values of the magnetic and electric fields:

$$H_x\big|_{i,j,k}^{n+1/2} = H_{x1}\big|_{i,j,k} H_x\big|_{i,j,k}^{n-1/2} + H_{x2}\big|_{i,j,k} \left(E_y\big|_{i,j,k+1/2}^{n} - E_y\big|_{i,j,k-1/2}^{n} + E_z\big|_{i,j-1/2,k}^{n} - E_z\big|_{i,j+1/2,k}^{n} \right) \quad (3a)$$

$$H_y\big|_{i,j,k}^{n+1/2} = H_{y1}\big|_{i,j,k} H_y\big|_{i,j,k}^{n-1/2} + H_{y2}\big|_{i,j,k} \left(E_z\big|_{i+1/2,j,k}^{n} - E_z\big|_{i-1/2,j,k}^{n} + E_x\big|_{i,j,k-1/2}^{n} - E_x\big|_{i,j,k+1/2}^{n} \right) \quad (3b)$$

$$H_z\big|_{i,j,k}^{n+1/2} = H_{z1}\big|_{i,j,k} H_z\big|_{i,j,k}^{n-1/2} + H_{z2}\big|_{i,j,k} \left(E_x\big|_{i,j+1/2,k}^{n} - E_x\big|_{i,j-1/2,k}^{n} + E_y\big|_{i-1/2,j,k}^{n} - E_y\big|_{i+1/2,j,k}^{n} \right) \quad (3c)$$

Determine electric field at integer temporal grid using the past values of the magnetic and electric fields:

$$E_x\big|_{i,j,k}^{n+1} = E_{x1}\big|_{i,j,k} E_x\big|_{i,j,k}^{n} + E_{x2}\big|_{i,j,k} \left(H_z\big|_{i,j+1/2,k}^{n+1/2} - H_z\big|_{i,j-1/2,k}^{n+1/2} + H_y\big|_{i,j,k-1/2}^{n+1/2} - H_y\big|_{i,j,k+1/2}^{n+1/2} \right) \quad (3d)$$

$$E_y\big|_{i,j,k}^{n+1} = E_{y1}\big|_{i,j,k} E_y\big|_{i,j,k}^{n} + E_{y2}\big|_{i,j,k} \left(H_x\big|_{i,j,k+1/2}^{n+1/2} - H_x\big|_{i,j,k-1/2}^{n+1/2} + H_z\big|_{i-1/2,j,k}^{n+1/2} - H_z\big|_{i+1/2,j,k}^{n+1/2} \right) \quad (3e)$$

$$E_z\big|_{i,j,k}^{n+1} = E_{z1}\big|_{i,j,k} E_z\big|_{i,j,k}^{n} + E_{z2}\big|_{i,j,k} \left(H_y\big|_{i+1/2,j,k}^{n+1/2} - H_y\big|_{i-1/2,j,k}^{n+1/2} + H_x\big|_{i,j-1/2,k}^{n+1/2} - H_x\big|_{i,j+1/2,k}^{n+1/2} \right) \quad (3f)$$

The sources may then be added as described by Eqs. (2). The electric-field updating coefficients are defined by material properties in the form

$$E_{x1}\big|_{i,j,k} = \frac{1 - \sigma_{i,j,k}\Delta t/(2\varepsilon_{i,j,k})}{1 + \sigma_{i,j,k}\Delta t/(2\varepsilon_{i,j,k})}, \quad E_{x2}\big|_{i,j,k} = \frac{\Delta t/(\varepsilon_{i,j,k}\Delta)}{1 + \sigma_{i,j,k}\Delta t/(2\varepsilon_{i,j,k})} \quad (3g)$$

The same equation applies to E_{y1}, E_{y2} and to E_{z1}, E_{z2}, respectively, but the material properties at the observation node *i,j,k* may be different.

The magnetic-field updating coefficients are defined by material properties in the similar form

$$H_{x1}\big|_{i,j,k} = \frac{1 - \overline{\rho}_{i,j,k}\Delta t/(2\mu_{i,j,k})}{1 + \overline{\rho}_{i,j,k}\Delta t/(2\mu_{i,j,k})}, \quad H_{x2}\big|_{i,j,k} = \frac{\Delta t/(\mu_{i,j,k}\Delta)}{1 + \overline{\rho}_{i,j,k}\Delta t/(2\mu_{i,j,k})} \quad (3h)$$

The same equation applies to H_{y1}, H_{y2} and to H_{z1}, H_{z2}, but the material properties at the observation node *i,j,k* may be different.

3.2. Numerical (integer spatial indexes) formulation

It is indeed convenient to use global integer indexes for programming purposes. The corresponding numbering scheme is shown in Fig. 2. Here, $G_{i,j,k}$ denotes the reference cube node.

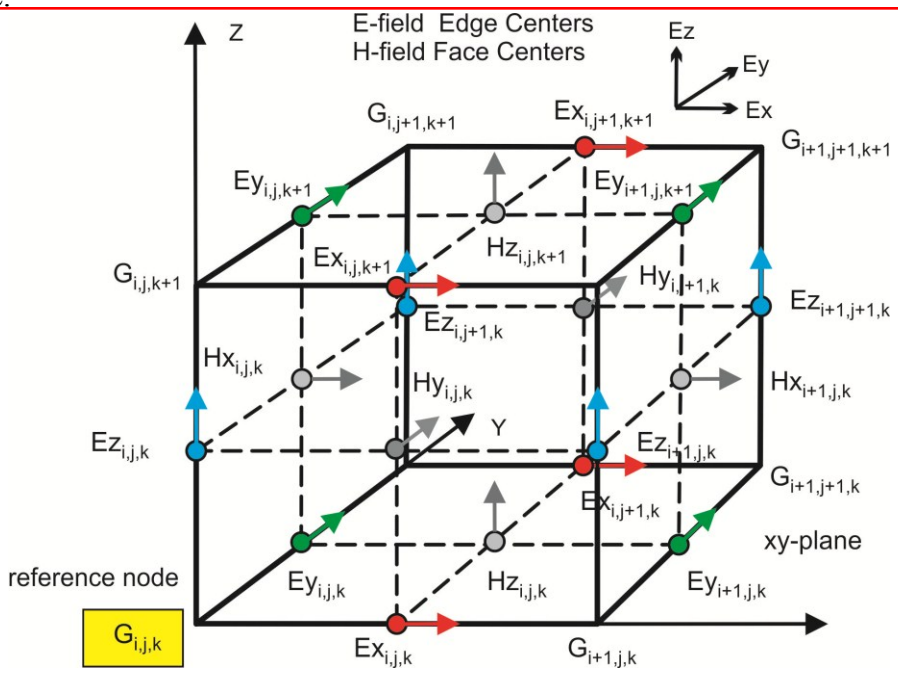

Fig. 2. A numbering scheme suitable for programming.

Eqs. (3) may be rewritten in terms of integer indexes. In short, ±½ is replaced by 1 or 0 in the magnetic field update equations, and ±½ is replaced by 0 or -1 in the electric field update equations, respectively. With reference to Fig. 2 one has

$$H_x\big|_{i,j,k}^{n+1/2} = H_{x1}\big|_{i,j,k} H_x\big|_{i,j,k}^{n-1/2} + H_{x2}\big|_{i,j,k} \left(E_y\big|_{i,j,k+1}^{n} - E_y\big|_{i,j,k}^{n} + E_z\big|_{i,j,k}^{n} - E_z\big|_{i,j+1,k}^{n} \right) \tag{4a}$$

$$H_y\big|_{i,j,k}^{n+1/2} = H_{y1}\big|_{i,j,k} H_y\big|_{i,j,k}^{n-1/2} + H_{y2}\big|_{i,j,k} \left(E_z\big|_{i+1,j,k}^{n} - E_z\big|_{i,j,k}^{n} + E_x\big|_{i,j,k}^{n} - E_x\big|_{i,j,k+1}^{n} \right) \tag{4b}$$

$$H_z\big|_{i,j,k}^{n+1/2} = H_{z1}\big|_{i,j,k} H_z\big|_{i,j,k}^{n-1/2} + H_{z2}\big|_{i,j,k} \left(E_x\big|_{i,j+1,k}^{n} - E_x\big|_{i,j,k}^{n} + E_y\big|_{i,j,k}^{n} - E_y\big|_{i+1,j,k}^{n} \right) \tag{4c}$$

Determine electric field at integer temporal grid using the past values of the magnetic and electric fields:

$$E_x\big|_{i,j,k}^{n+1} = E_{x1}\big|_{i,j,k} E_x\big|_{i,j,k}^{n} + E_{x2}\big|_{i,j,k} \left(H_z\big|_{i,j,k}^{n+1/2} - H_z\big|_{i,j-1,k}^{n+1/2} + H_y\big|_{i,j,k-1}^{n+1/2} - H_y\big|_{i,j,k}^{n+1/2} \right) \tag{4d}$$

$$E_y\big|_{i,j,k}^{n+1} = E_{y1}\big|_{i,j,k} E_y\big|_{i,j,k}^{n} + E_{y2}\big|_{i,j,k} \left(H_x\big|_{i,j,k}^{n+1/2} - H_x\big|_{i,j,k-1}^{n+1/2} + H_z\big|_{i-1,j,k}^{n+1/2} - H_z\big|_{i,j,k}^{n+1/2} \right) \tag{4e}$$

$$E_z\big|_{i,j,k}^{n+1} = E_{z1}\big|_{i,j,k} E_z\big|_{i,j,k}^{n} + E_{z2}\big|_{i,j,k}\left(H_y\big|_{i,j,k}^{n+1/2} - H_y\big|_{i-1,j,k}^{n+1/2} + H_x\big|_{i,j-1,k}^{n+1/2} - H_x\big|_{i,j,k}^{n+1/2}\right) \tag{4f}$$

The electric-field updating coefficients are defined by material properties in the same form as before

$$E_{x1}\big|_{i,j,k} = \frac{1-\sigma_{i,j,k}\Delta t/(2\varepsilon_{i,j,k})}{1+\sigma_{i,j,k}\Delta t/(2\varepsilon_{i,j,k})}, \quad E_{x2}\big|_{i,j,k} = \frac{\Delta t/(\varepsilon_{i,j,k}\Delta)}{1+\sigma_{i,j,k}\Delta t/(2\varepsilon_{i,j,k})} \tag{4g}$$

The same equation applies to E_{y1}, E_{y2} and to E_{z1}, E_{z2}, respectively, but the material properties at the observation node *i,j,k* may be different.

The magnetic-field updating coefficients are defined by material properties in the same form as before

$$H_{x1}\big|_{i,j,k} = \frac{1-\overline{\rho}_{i,j,k}\Delta t/(2\mu_{i,j,k})}{1+\overline{\rho}_{i,j,k}\Delta t/(2\mu_{i,j,k})}, \quad H_{x2}\big|_{i,j,k} = \frac{\Delta t/(\mu_{i,j,k}\Delta)}{1+\overline{\rho}_{i,j,k}\Delta t/(2\mu_{i,j,k})} \tag{4h}$$

The same equation applies to H_{y1}, H_{y2} and to H_{z1}, H_{z2}, but the material properties at the observation node *i,j,k* may be different.

4. Exponential time stepping

For a medium with high loss the update coefficients in Eqs. (4g), (4h) may become negative. This leads to a numerical instability. A solution to this problem is to "pre-solve" Maxwell's curl equations, by first finding the solution of homogeneous equations, say

$$\varepsilon\frac{\partial\vec{E}}{\partial t} = -\sigma\vec{E} \rightarrow \vec{E}_{\text{hom}}(t) = \vec{E}^{0}_{\text{hom}}\exp(-\sigma t/\varepsilon) \tag{5a}$$

and then obtain the solution of the full equations in the form of a convolution integral. This results in the following formulas for the update coefficients, valid for both homogeneous and inhomogeneous materials [6]

$$\begin{aligned} E_{x1}\big|_{i,j,k} &= \frac{1-\sigma_{i,j,k}\Delta t/(2\varepsilon_{i,j,k})}{1+\sigma_{i,j,k}\Delta t/(2\varepsilon_{i,j,k})} \rightarrow \exp\left(-\sigma_{i,j,k}\Delta t/\varepsilon_{i,j,k}\right) \\ E_{x2}\big|_{i,j,k} &= \frac{\Delta t/(\varepsilon_{i,j,k}\Delta)}{1+\sigma_{i,j,k}\Delta t/(2\varepsilon_{i,j,k})} \rightarrow \frac{1}{\sigma\Delta}\left(1-\exp\left(-\sigma_{i,j,k}\Delta t/\varepsilon_{i,j,k}\right)\right) \end{aligned} \tag{5b}$$

The same equation applies to E_{y1}, E_{y2} and to E_{z1}, E_{z2}, respectively, but the material properties at the observation node *i,j,k* may be different. Eqs. (5b) are equivalent to Taylor series to the first or second order of accuracy.

The magnetic-field updating coefficients are modified accordingly

$$H_{x1}\big|_{i,j,k} = \frac{1-\bar{\rho}_{i,j,k}\Delta t/(2\mu_{i,j,k})}{1+\bar{\rho}_{i,j,k}\Delta t/(2\mu_{i,j,k})} \to \exp\left(-\bar{\rho}_{i,j,k}\Delta t/\mu_{i,j,k}\right)$$
$$H_{x2}\big|_{i,j,k} = \frac{\Delta t/(\mu_{i,j,k}\Delta)}{1+\bar{\rho}_{i,j,k}\Delta t/(2\mu_{i,j,k})} \to \frac{1}{\bar{\rho}\Delta}\left(1-\exp\left(-\bar{\rho}_{i,j,k}\Delta t/\mu_{i,j,k}\right)\right) \quad (5c)$$

The same equation applies to H_{y1}, H_{y2} and to H_{z1}, H_{z2}, but the material properties at the observation node i,j,k may be different. Eqs. (5b) are again equivalent to Taylor series to the first or second order of accuracy.

The implementation of the exponential time stepping requires care, due to the singularity of the second Eq. (5b) when $\sigma \to 0$. A vanishingly small conductivity value for air, that is $\sigma = 10^{-6}$ S/m , was assumed to make second Eq. (5b) uniformly valid.

The exponential time stepping may be applied to problems involving highly-conductive dielectrics – human body, salt water, Earth ground – at low and intermediate frequencies. It can be also applied to the direct modeling of metal objects by imposing a very high conductivity in the object volume.

5. MATLAB implementation of the Yee method

The MATLAB implementation of Eqs. (4) is surprisingly simple. One version utilizing the function `diff` is given here [5]. We assume that the FDTD cubic grid has $N_x \times N_y \times N_z$ cube cells and $(N_x+1)\times(N_y+1)\times(N_z+1)$ corner nodes. The dimensions of field arrays are given by

```
% Allocate field matrices
Ex = zeros(Nx  , Ny+1, Nz+1);
Ey = zeros(Nx+1, Ny  , Nz+1);
Ez = zeros(Nx+1, Ny+1, Nz  );
Hx = zeros(Nx+1, Ny  , Nz  );
Hy = zeros(Nx  , Ny+1, Nz  );
Hz = zeros(Nx  , Ny  , Nz+1);
```

For the electric field, the update equations have the form

```
%%  E-field update (everywhere except on the boundary
ExN(:,2:Ny,2:Nz) = Ex1.*ExP(:,2:Ny,2:Nz)+Ex2.*(diff(HzP(:,:,2:Nz),1,2)-diff(HyP(:,2:Ny,:),1,3));
EyN(2:Nx,:,2:Nz) = Ey1.*EyP(2:Nx,:,2:Nz)+Ey2.*(diff(HxP(2:Nx,:,:),1,3)-diff(HzP(:,:,2:Nz),1,1));
EzN(2:Nx,2:Ny,:) = Ez1.*EzP(2:Nx,2:Ny,:)+Ez2.*(diff(HyP(:,2:Ny,:),1,1)-diff(HxP(2:Nx,:,:),1,2));
```

For the magnetic field, one similarly has

```
%%  H-field update (everywhere)
HxN =  Hx1.*HxP + Hx2.*(diff(EyN,1,3)- diff(EzN,1,2));
HyN =  Hy1.*HyP + Hy2.*(diff(EzN,1,1)- diff(ExN,1,3));
HzN =  Hz1.*HzP + Hz2.*(diff(ExN,1,2)- diff(EyN,1,1));
```

No other update equations except the boundary become necessary.

6. References

[1]. K. S. Yee, "Numerical solution of initial boundary value problem involving Maxwell's equations in isotropic media," *IEEE Trans. Antennas and Propagation*, vol. 14, 1966, pp. 302-307.

[2]. C. A. Balanis, *Advanced Engineering Electromagnetics*, Wiley, New York, 1989.

[3]. R. F. Harrington, *Time-Harmonic Electromagnetic Fields*, McGraw Hill, New York, 1961.

[4]. A. Taflove, *Computational Electrodynamics, The Finite Difference Time Domain Approach*, Third Ed., Artech House, Norwood, MA, 2005.

[5]. A. Bondeson, T. Rylander, and P. Ingelström, *Computational Electromagnetics*, Springer, New York, 2005, Series: Texts in Applied Mathematics , Vol. 51., pp. 58-86.

[6]. R. Holland, "Finite-difference time-domain (FDTD) analysis of magnetic diffusion," *IEEE Trans. Electromagnetic Compatibility*, vol. 36, pp. 32-39, Feb. 1994.

Section II. Material properties

1. Material properties

In the standard FDTD formulation, every elementary Yee cell (electric-field components along a cube edges) is filled by a homogeneous medium. Dielectric boundaries can be only located between adjacent cells, therefore, they are tangential to the electric field components – see Fig. 3. Simultaneously, magnetic boundaries can be only located halfway between adjacent cells, therefore they are also tangential to the magnetic field components. Fig. 3 shows the corresponding concept.

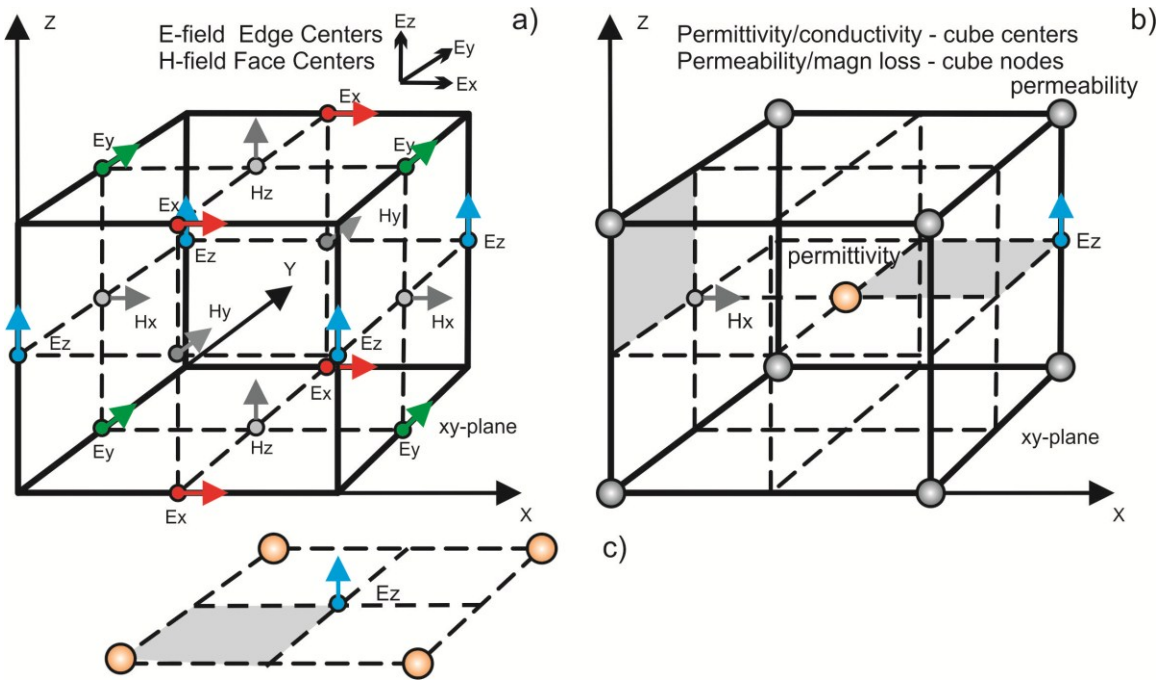

Fig. 3. Standard field nodes and material parameter nodes. The permittivity/conductivity is defined at cell centers. The permeability/magnetic loss is defined at cell corners.

Effective constitutive parameters are derived by enforcing the continuity of the tangential electric- and magnetic field components in the integral formulation of the Ampere's law and Faraday's law [1]. These parameters are obtained by averaging the parameters of the neighboring cells with respect to the discontinuity. Such formulation is first-order accurate in cell size and leads to the definition of an effective permittivity and permeability. The result has the form[1],[2]:

- $\varepsilon_{i,j,k}, \sigma_{i,j,k}$ in Eqs. (4a) are obtained by averaging *four* adjacent center-cell values –see Fig. 2c;
- $\mu_{i,j,k}, \bar{\rho}_{i,j,k}$ in Eqs. (4b) are obtained by averaging *four* adjacent node values.

2. MATLAB implementation

We assume again that the FDTD cubic grid has $N_x \times N_y \times N_z$ cube cells and $(N_x+1)\times(N_y+1)\times(N_z+1)$ corner nodes. Then, the dielectric properties are described by 3D permittivity and conductivity arrays initialized in the form

```
DIELC    = ones(Nx, Ny, Nz);  %3D Permittivity array  on half grid (cube centers)
SIGEC    = zeros(Nx, Ny, Nz); %3D Electric conductivity array on half grid (cube centers)
```

Once those arrays have been filled, the electric-field updating coefficients from Eq. (4a) are defined by material properties in the form (the result is only given for E_{z1}, E_{z2}, other coefficient are obtained by permutation)

```
%   Arrays for Ez
nx = 2:Nx; ny = 2:Ny; nz =2:Nz;
Dtemp = (DIELC(nx,ny,:)+DIELC(nx-1,ny,:)+DIELC(nx,ny-1,:)+DIELC(nx-1,ny-1,:))/4;
Stemp = (SIGEC(nx,ny,:)+SIGEC(nx-1,ny,:)+SIGEC(nx,ny-1,:)+SIGEC(nx-1,ny-1,:))/4;

    Ez1     = (1 - dt*Stemp./(2*Dtemp))./(1 + dt*Stemp./(2*Dtemp));
    Ez2     = (dt./(d*Dtemp))./(1 + dt*Stemp./(2*Dtemp));
    Ez1     = Ez1(:, :, nz);
    Ez2     = Ez2(:, :, nz);
```

The exponential time-stepping considered in the previous section requires the somewhat different update:

```
    Stemp   = Stemp + 1e-9;
    Ez1     = exp(-dt*Stemp./Dtemp);
    Ez2     = (1 - exp(-dt*Stemp./Dtemp))./(d*Stemp);
    Ez1     = Ez1(:, :, nz);
    Ez2     = Ez2(:, :, nz);
```

Similarly, for the magnetic field one initializes 3D permeability and resistivity arrays with the dimensions given by

```
MAGNC  = ones(Nx+1, Ny+1, Nz+1); %3D Permeability array on integer grid (cube nodes)
RHOMC  = zeros(Nx+1,Ny+1, Nz+1); %3D Magnetic res. array on integer grid (cube nodes)
```

The magnetic-field updating coefficients from Eq. (4b) have the form (the result is only given for H_{x1}, H_{x2}, other coefficient are obtained by permutation)

```
ny = 1:Ny; nz = 1:Nz;
Mtemp = (MAGNC(:,ny,nz)+MAGNC(:,ny+1,nz)+MAGNC(:,ny,nz+1)+MAGNC(:,ny+1,nz+1))/4;
Rtemp = (RHOMC(:,ny,nz)+RHOMC(:,ny+1,nz)+RHOMC(:,ny,nz+1)+RHOMC(:,ny+1,nz+1))/4;

    Hx1  = (1 - dt*Rtemp./(2*Mtemp))./(1 + dt*Rtemp./(2*Mtemp));
    Hx2  = (dt./(d*Mtemp))./(1 + dt*Rtemp./(2*Mtemp));
```

The exponential time-stepping considered in the previous section requires the somewhat different update:

```
Rtemp   = Rtemp + 1e-9;
Hx1     = exp(-dt*Rtemp./Mtemp);
Hx2     = (1 - exp(-dt*Rtemp./Mtemp))./(d*Rtemp + eps);
```

More accurate (subcell) models of fine dielectric and magnetic boundaries crossing the unit cells are possible at the expense of increased complexity [3].

3. References

[1]. G. Marrocco, M. Sabbadini, and F. Bardati, "FDTD Improvement by Dielectric Subgrid Resolution," IEEE Trans. Microwave Theory Techniques, vol. 46, no. 12, Dec. 1998, pp. 2166-2169.

[2]. K. S. Kunz and R. Luebbers, *The Finite Difference Time Domain Method*, Boca Raton, FL: CRC Press, 1993.

[3]. A. Taflove, *Computational Electrodynamics, The Finite Difference Time Domain Approach*, Third Ed., Artech House, Norwood, MA, 2005, Chapter 10.

Section III. Model of a small dipole antenna (electric dipole)

1. Standard small dipole model (center of dipole is on node of E)

A small dipole antenna is represented by a uniform line current, $i_s(t)$, which flows over a length l. The length l is usually much smaller than the cell size. The current is centered at the corresponding electric field node as shown in Fig. 5 (see, for example, [1]).

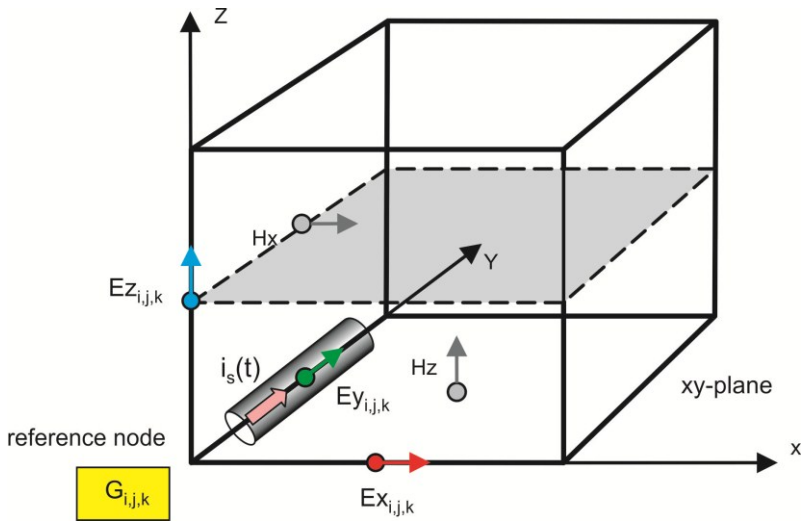

Fig. 5. Dipole antenna with the impressed line current $i_s(t)$.

The line current is transformed to an equivalent volumetric current density averaged over one unit cell:

$$J_s(t) = \frac{l}{\Delta^3} i_s(t) \tag{1}$$

which produces the same electric dipole moment. This current density is substituted in one of the FDTD update equations for the electric field (Eqs. (4d) to (4f)). For the dipole shown in Fig. 5, the result has the form

$$E_y^{n+1}(i,j,k) = E_{y1}E_y^n(i,j,k) + E_{y2}\times \\ \left(H_x^{n+1/2}(i,j,k) - H_x^{n+1/2}(i,j,k-1) + H_z^{n+1/2}(i-1,j,k) - H_z^{n+1/2}(i,j,k) - \Delta J_s^{n+1/2}\right) \quad (2)$$

where

$$E_{x1} = \frac{1-\sigma\Delta t/(\varepsilon\Delta)}{1+\sigma\Delta t/(2\varepsilon)}, \quad E_{x2}\big|_{i,j,k} = \frac{\Delta t/(\varepsilon\Delta)}{1+\sigma\Delta t/(2\varepsilon)} \quad (3)$$

An important observation is that it is very straightforward to implement Eqs. (2) in practice. Namely, only current excitation terms have to be added after the standard update equations for the electric field.

2. Small dipole model for arbitrary orientation (center of dipole is on corner node)

2 rahe hale in halat

For an arbitrarily oriented dipole, with the unit direction vector $\vec{n}$, one could consider a superposition solution in the form of three orthogonal elementary dipoles oriented along the *x*-, *y*-, and *z*-axes. However, their phase centers will not be coincident – see Fig. 5 for an illustration. A modification of the model can be made that is shown in Fig. 6. Here, the dipole source is effectively placed at the corner node of the Yee cell. Two adjacent electric field nodes acquire the half of the dipole current.

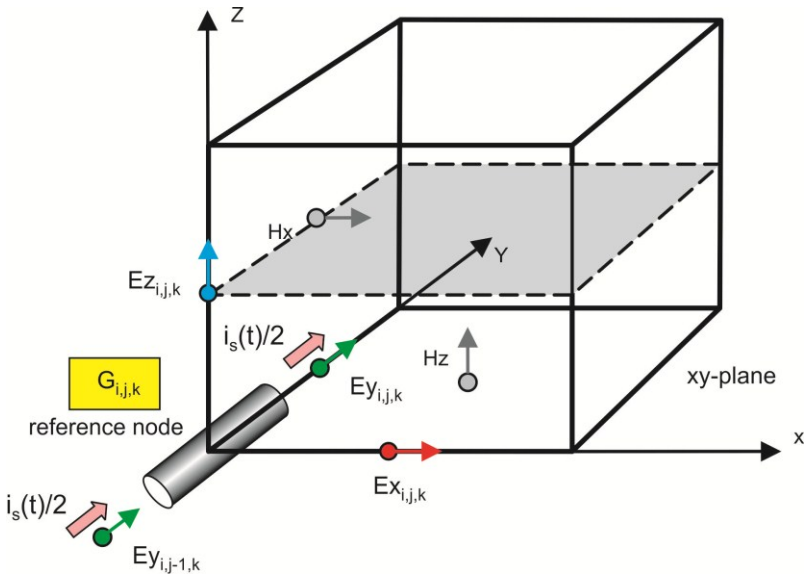

Fig. 6. Dipole antenna model with the dipole placed at the center node of the Yee cell.

The dipole of arbitrary orientation with the unit direction vector $\vec{n}$ is then considered as a superposition of three dipoles directed along the *x*-, *y*-, and *z*-axes. All those dipoles have the same (phase) center. The corresponding current densities are given by

$$J_{sX}(t) = \frac{1}{2}n_X i_s(t), \quad J_{sY}(t) = \frac{1}{2}n_Y i_s(t), \quad J_{sZ}(t) = \frac{1}{2}n_Z i_s(t) \quad (4)$$

The above model may be treated as a *symmetric* point source model.

The port update given Eq. (2) is straightforwardly modified to the present case: it remains the same for the node i, j, k (except that the current is divided by two), and uses index substitution $j \to j-1$ for the second node in Fig. 6.

Complete update equations for a dipole of arbitrary orientation have the form

$$\begin{aligned}
&E_x^{n+1}(i,j,k) \to E_x^{n+1}(i,j,k) - E_{x2}(0.5\Delta n_z J_s^{n+1/2}) \\
&E_x^{n+1}(i-1,j,k) \to E_x^{n+1}(i-1,j,k) - E_{x2}(0.5\Delta n_z J_s^{n+1/2}) \\
&E_y^{n+1}(i,j,k) \to E_y^{n+1}(i,j,k) - E_{y2}(0.5\Delta n_Y J_s^{n+1/2}) \\
&E_y^{n+1}(i,j-1,k) \to E_y^{n+1}(i,j-1,k) - E_{y2}(0.5\Delta n_Y J_s^{n+1/2}) \\
&E_z^{n+1}(i,j,k) \to E_z^{n+1}(i,j,k) - E_{z2}(0.5\Delta n_z J_s^{n+1/2}) \\
&E_z^{n+1}(i,j,k-1) \to E_z^{n+1}(i,j,k-1) - E_{z2}(0.5\Delta n_z J_s^{n+1/2})
\end{aligned} \tag{5}$$

Here, only current excitation terms have to be added after the standard update equations for the electric field.

The model described above was implemented in the code. It is advantage is the ability to describe the coil of arbitrary orientation, whilst keeping the same phase center. Its disadvantage is a "large" volume occupied by the coil model that extends to two unit cells in every direction.

3. Pulse form to be used

In general, the pulse form may be chosen arbitrarily. A (default) bipolar Gaussian (Rayleigh) current pulse used in the examples has the form

$$i_s(t) = I_0 \frac{(t_0 - t)}{\tau} \exp\left(\frac{-(t-t_0)^2}{(2\tau)^2}\right), \quad t_0 = 5\tau \tag{6}$$

Its center frequency and a 3dB-power bandwidth are given by

$$f_c = \frac{0.16}{\tau}, \qquad \mathrm{BW} = 1.15 f_c \tag{7}$$

For example,

$$\tau = 0.4\mathrm{ns}, \quad \tau = 0.2\mathrm{ns}, \quad \tau = 0.1\mathrm{ns}; \Rightarrow f_c = 400\,\mathrm{MHz}, \quad f_c = 800\,\mathrm{MHz}, \quad f_c = 1.6\,\mathrm{GHz} \tag{8}$$

4. MATLAB implementation

The MATLAB implementation of the symmetric dipole model (and of the related field probe) is given by the code that follows

```
%   setting up parameters
Js   = PortM(m)/d^3*(IG(m, kt)+IG(m, kt+1))/2;% volum. current density at n+1/2
i_e = PortIndX(m);   %   port location grid nodes
j_e = PortIndY(m);   %   port location grid nodes
k_e = PortIndZ(m);   %   port location grid nodes
Jx = d*Js/2*PortNX(m);
Jy = d*Js/2*PortNY(m);
Jz = d*Js/2*PortNZ(m);

ExN(i_e, j_e, k_e)   = ExN(i_e, j_e, k_e)   - Ex2(i_e, j_e-1, k_e-1)*Jx;
ExN(i_e-1, j_e, k_e) = ExN(i_e-1, j_e, k_e) - Ex2(i_e-1, j_e-1, k_e-1)*Jx;

EyN(i_e, j_e, k_e)   = EyN(i_e, j_e, k_e)   - Ey2(i_e-1, j_e, k_e-1)*Jy;
EyN(i_e, j_e-1, k_e) = EyN(i_e, j_e-1, k_e) - Ey2(i_e-1, j_e-1, k_e-1)*Jy;

EzN(i_e, j_e, k_e)   = EzN(i_e, j_e, k_e)   - Ez2(i_e-1, j_e-1, k_e)*Jz;
EzN(i_e, j_e, k_e-1) = EzN(i_e, j_e, k_e-1) - Ez2(i_e-1, j_e-1, k_e-1)*Jz;

AntI(m, kt) = IG(m, kt);

AntE(m, kt) = PortNX(m)*(ExP(i_e, j_e, k_e) + ExP(i_e-1, j_e, k_e)) + ...
              PortNY(m)*(EyP(i_e, j_e, k_e) + EyP(i_e, j_e-1, k_e)) + ...
              PortNZ(m)*(EzP(i_e, j_e, k_e) + EzP(i_e, j_e, k_e-1));
AntE(m, kt) = AntE(m, kt)/2;
                                                    %   at step n - tested

AntH(m, kt) = PortNX(m)*(HxN(i_e, j_e, k_e) + HxN(i_e, j_e-1, k_e) + HxN(i_e,
j_e, k_e-1) + HxN(i_e, j_e-1, k_e-1)) + ...
              PortNY(m)*(HyN(i_e, j_e, k_e) + HyN(i_e-1, j_e, k_e) + HyN(i_e,
j_e, k_e-1) + HyN(i_e-1, j_e, k_e-1)) + ...
              PortNZ(m)*(HzN(i_e, j_e, k_e) + HzN(i_e-1, j_e, k_e) + HzN(i_e,
j_e-1, k_e) + HzN(i_e-1, j_e-1, k_e)) + ...
              PortNX(m)*(HxP(i_e, j_e, k_e) + HxP(i_e, j_e-1, k_e) + HxP(i_e,
j_e, k_e-1) + HxP(i_e, j_e-1, k_e-1)) + ...
              PortNY(m)*(HyP(i_e, j_e, k_e) + HyP(i_e-1, j_e, k_e) + HyP(i_e,
j_e, k_e-1) + HyP(i_e-1, j_e, k_e-1)) + ...
              PortNZ(m)*(HzP(i_e, j_e, k_e) + HzP(i_e-1, j_e, k_e) + HzP(i_e,
j_e-1, k_e) + HzP(i_e-1, j_e-1, k_e));
AntH(m, kt) = AntH(m, kt)/8;
```

The accuracy and limitations of the small symmetric-dipole model have been quantified by many examples using the comparison with analytical solutions for point sources [2] reformulated in time domain.

References

[1]. R. Pontalti, J. Nadobny, P. Wust, A. Vaccari, and D. Sullivan, “Investigation of Static and Quasi-Static Fields Inherent to the Pulsed FDTD Method,” *IEEE Trans. Microwave Theory Techniques*, vol. 50, no 8, Aug. 2002, pp. 2022-2025.

[2]. C. A. Balanis, *Antenna Theory. Analysis and Design*, Third Ed., Wiley, New York, 2005, Chapter 5.

Section IV. Model of a small coil antenna (magnetic dipole)

1. General facts about coil antennas

Consider a coil antenna with the dimensions shown in Fig. 7. The antenna has N turns; the coil cross-section is A; the length is l. The antenna is oriented along the z-axis. The coil may have a finite magnetic core.

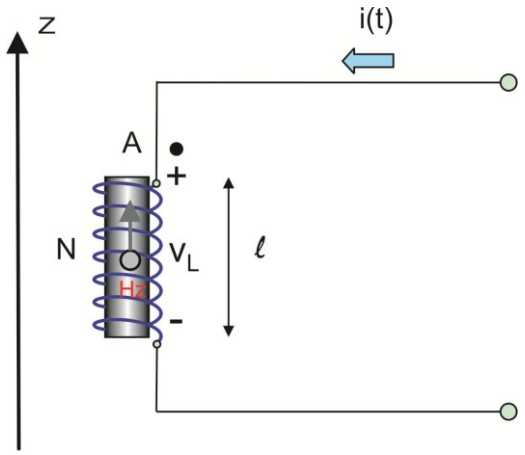

Fig.7. A coil antenna (with or without) the magnetic core.

The antenna is excited by a current pulse $i(t)$. If necessary, the voltage across the coil antenna may be calculated by [1]

$$\upsilon_L(t) = L\frac{di}{dt} + Ri, \quad L = L_{\text{static}}, \quad R = R_{\text{static}} + R_{\text{rad}} \tag{1}$$

where two indexes relate to static values and their radiation corrections, respectively. One has for the static inductance of an air-core solenoid with radius r , cross-section area A, and length l,

$$L_{\text{static}} = \frac{\mu_0 A N^2}{l}\left(1 - \frac{8\text{w}}{3\pi} + \frac{\text{w}^2}{2} - \frac{\text{w}^4}{4}\right), \quad \text{w} = \frac{r}{l} < 1 \tag{2}$$

The radiation resistance is given by [1]

$$R_{\text{rad}} = \frac{\eta_0}{6\pi}\left(\frac{\omega}{c_0}\right)^4 (AN)^2 \tag{3}$$

The radiation resistance is negligibly small for very small coils.

The calculation of inductance for the coil with a straight magnetic core becomes a nontrivial theoretical exercise. The graphical data is given in [1]. We also present here a useful theoretical result. It is only valid for a high-permeability magnetic core, with approximately $\mu \geq 100\,\mu_0$. The resulting inductance for the inductor in Fig. 7 has the form [2]

$$L = \frac{0.5\pi\mu_0 l^* N^2}{\ln\left[\dfrac{l^*}{r} - 1\right]}\left(1 - \frac{l}{2l^*}\right) \quad \text{[H]} \tag{4}$$

where l^* is the core length and r is the coil radius. Interestingly, the resulting inductance does not explicitly depend on the specific value of μ as long as this value is sufficiently large. More precisely, Eq. (4) holds only for situations where the core length-to-diameter ratio is considerably smaller than the relative magnetic permeability, $\mu_r = \mu/\mu_0$. Eq. (4) was compared with experiment and indicated about 40% accuracy in predicting the inductance.

2. Receive coil

2.1. Coil without magnetic core

In the receiving mode, the open-circuited air-core RX coil shown in Fig. 7 generates the induced emf voltage,

$$E_{emf}(t) = -\mu_0 AN \frac{\partial H_z}{\partial t} \tag{5a}$$

where the emf polarity "+" corresponds to the dotted terminal of the coil shown in Fig. 7. Thus, the receive coil in the open-circuit mode does not significantly disturb the incident field and acts *similar* to a field probe. This concept will be implemented in the numerical code. Therefore, the small receive coil does not need a dedicated FDTD modeling.

In terms of finite differences, one has

$$E_{emf}^n = -\frac{\mu_0 AN}{\Delta t}\left(H_z^{n+1/2}(i,j,k) - H_z^{n-1/2}(i,j,k)\right) \tag{5b}$$

An alternative is to use Eq. (10) with zero sources, which yields

$$E_{emf}(t) = AN\left(\nabla \times \vec{E}\right)_z \Rightarrow E^n_{emf} = AN\left(\nabla \times \vec{E}\right)^n_z \tag{5c}$$

The Yee-grid discretization gives

$$\left(\nabla \times \vec{E}\right)^n_z = -1/(\Delta)\left(E^n_x(i,j+1,k) - E^n_x(i,j,k) + E^n_y(i,j,k) - E^n_y(i+1,j,k)\right) \tag{5d}$$

2.2. Coil with arbitrary orientation

In this case, Eq. (5) is modified to

$$E_{emf}(t) = -\mu_0 AN \frac{\partial \vec{H}}{\partial t} \cdot \vec{n} = -\mu_0 AN \frac{\partial \vec{H} \cdot \vec{n}}{\partial t} \tag{6}$$

where $\vec{n}$ is the unit vector in the direction of the coil axis, directed toward the dotted terminal of the coil in Fig. 7. Eqs. (5b) through (5c) may be modified accordingly.

2.3. Coil with a magnetic core

For the coil with the core, the situation complicates. Comparing Eq. (2) (with $w \to 0$) and Eq. (4) one could in principle define the "effective" permeability within the coil, i.e. the permeability, which gives the same inductance, in the form,

$$\mu_{eff} = \frac{0.5\mu_0 l^* l}{\ln\left[\frac{l^*}{r} - 1\right] r^2}\left(1 - \frac{l}{2l^*}\right) \tag{7}$$

Herewith, the induced emf voltage might be defined in the form

$$E_{emf}(t) = -\mu_{eff} AN \frac{\partial \vec{H} \cdot \vec{n}}{\partial t} \tag{8}$$

Eq. (8) was not tested by comparison with experiment and should be used with care.

3. Transmit coil - a magnetic dipole

3.1 Magnetic dipole

A small transmit coil antenna which carries the current $i(t)$ in Fig. 7 is modeled as an infinitesimally small magnetic dipole with a *magnetic moment* $M_z(t)$. For the coil without the magnetic core,

$$M_z(t) = ANi(t) \tag{9}$$

where A is the coil cross-section, N is the number of turns, and $i(t)$ is the instantaneous coil current. The meaning of the magnetic moment originates from the torque exerted on a loop of current in an external magnetic field. On the other hand, the magnetic moment is the only characteristic of a very small coil antenna that defines both its near- and far field [3],[4]. Generally, the magnetic moment is a vector quantity, with the unit direction vector $\vec{n}$. The magnetic moment is directed along the coil axis according to the right-hand rule for the electric current. For example, it is directed up in Fig. 7.

3.2 Magnetic dipole model with a magnetic current source

The simplest way to model the coil antenna is to introduce the magnetic current source density into Faraday's law Eq. (2b)

$$\mu \frac{\partial \vec{H}}{\partial t} = -\nabla \times \vec{E} - \vec{J}_m - \vec{n} J_{ms} \tag{10}$$

$$J_{ms}(\vec{r},t) = \mu_0 \delta(\vec{r}) \frac{dM_z}{dt} \tag{11}$$

Averaging over the volume of the FDTD unit cell yields

$$J_{ms}(t) = \frac{\mu_0}{\Delta^3} \frac{dM_z}{dt} = \frac{\mu_0 AN}{\Delta^3} \frac{di}{dt} \tag{12}$$

The Yee-grid discretization yields

$$H_z^{n+1/2}(i,j,k) = H_z^{n-1/2}(i,j,k) + \Delta t/(\mu_0 \Delta)\left(E_x^n(i,j+1,k) - E_x^n(i,j,k) + E_y^n(i,j,k) - E_y^n(i+1,j,k)\right) - \frac{AN}{\Delta^3}\left(i^{n+1/2} - i^{n-1/2}\right) \tag{13}$$

This method has a number of disadvantages. One of them is that the magnetic current source given by Eqs. (12) and (13) does not work well on the boundary between vacuum and a magnetic material. Therefore, it is not implemented in the code.

3.3 Magnetic dipole model with a loop of electric current

The small coil antenna may be modeled with a loop of electric current – see Fig. 8. The coil antenna is placed at the node of the co-polar magnetic field as shown in Fig. 1. This is *not* the sub-cell model of the coil, but rather the cell model.

Such a location is convenient, but it does not allow us to consider an arbitrary coil antenna orientation in general. An arbitrarily-oriented radiating coil may be considered as a superposition of three coils oriented along the axes; however, these coils will not have the same phase center.

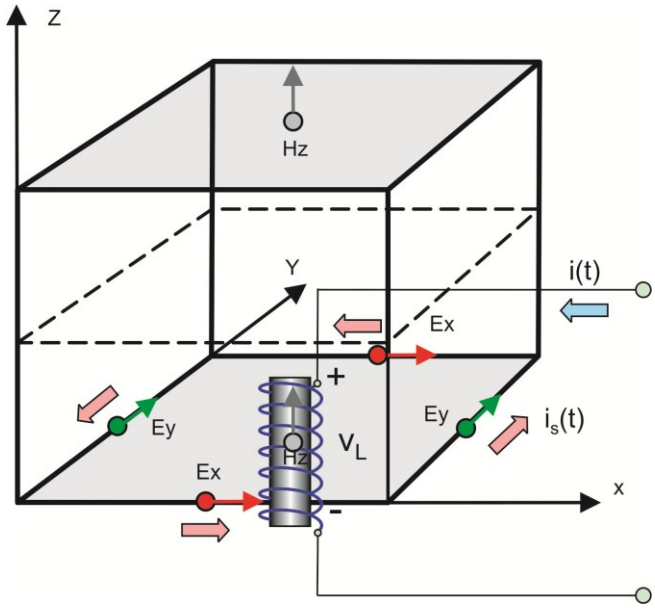

Fig. 8. Coil antenna modeled with a loop of an equivalent electric current.

Following the approach from Ref. [4], the coil in Fig. 8 is replaced by a square loop of the grid-aligned current $i_s(t)$ which possesses *the same* magnetic moment:

$$\Delta^2 i_s(t) = M_z(t) \Rightarrow i_s(t) = \frac{AN}{\Delta^2} i(t) \tag{14}$$

where Δ is the cell size of the cubic grid. Further, the current $i_s(t)$ is replaced by its current density uniformly distributed over every involved cell's cross-section,

$$J_s(t) = \frac{i_s(t)}{\Delta^2} \Rightarrow J_s(t) = \frac{AN}{\Delta^4} i(t) \tag{15}$$

Let's assume the coil is located at the H_z-field node i,j,k – see Fig. 8. Maxwell's equations in a lossy inhomogeneous medium for four surrounding E-field nodes

$$\varepsilon \frac{\partial \vec{E}}{\partial t} = \nabla \times \vec{H} - \sigma \vec{E} - \hat{z} J_s \tag{16}$$

on the Yee grid are modified to

$$\begin{aligned} &E_x^{n+1}(i,j,k) = E_{x1} E_x^n(i,j,k) + E_{x2} \times \\ &\left(H_z^{n+1/2}(i,j,k) - H_z^{n+1/2}(i,j-1,k) + H_y^{n+1/2}(i,j,k-1) - H_y^{n+1/2}(i,j,k) - \Delta J_s^{n+1/2} \right) \end{aligned} \tag{17a}$$

$$E_x^{n+1}(i,j+1,k) = E_{x1}E_x^n(i,j+1,k) + E_{x2}\times \\ \left(H_z^{n+1/2}(i,j+1,k) - H_z^{n+1/2}(i,j,k) + H_y^{n+1/2}(i,j+1,k-1) - H_y^{n+1/2}(i,j+1,k) + \Delta J_s^{n+1/2}\right) \quad (17b)$$

$$E_y^{n+1}(i,j,k) = E_{y1}E_y^n(i,j,k) + E_{y2}\times \\ \left(H_x^{n+1/2}(i,j,k) - H_x^{n+1/2}(i,j,k-1) + H_z^{n+1/2}(i-1,j,k) - H_z^{n+1/2}(i,j,k) + \Delta J_s^{n+1/2}\right) \quad (17c)$$

$$E_y^{n+1}(i+1,j,k) = E_{y1}E_y^n(i+1,j,k) + E_{y2}\times \\ \left(H_x^{n+1/2}(i+1,j,k) - H_x^{n+1/2}(i+1,j,k-1) + H_z^{n+1/2}(i,j,k) - H_z^{n+1/2}(i+1,j,k) - \Delta J_s^{n+1/2}\right) \quad (17d)$$

where

$$E_{x1} = \frac{1-\sigma\Delta t/(\varepsilon\Delta)}{1+\sigma\Delta t/(2\varepsilon)}, \quad E_{x2}\big|_{i,j,k} = \frac{\Delta t/(\varepsilon\Delta)}{1+\sigma\Delta t/(2\varepsilon)} \quad (18)$$

at the locations of the *E*-field nodes. Here, σ is the electric conductivity.

An important observation is that it is very straightforward to implement Eqs. (17) in practice. Namely, only current excitation terms have to be added after the standard update equations for the electric field.

3.4 Magnetic dipole model with two loops of electric current and arbitrary coil orientation

The current-loop model of Fig. 8 is straightforwardly modified for the case of arbitrary coil orientation. The concept is shown in Fig. 9 that follows. The coil antenna is now placed at the center of the Yee cell. The coil in Fig. 9 is replaced by *two* square loops of the grid-aligned electric current, which in sum possess the same magnetic moment. Instead of Eq. (15), the current density for each loop becomes

$$J_s(t) = \frac{1}{2}\frac{AN}{\Delta^4}i(t) \quad (19)$$

i.e. the half of the original current density. Update Eqs. (17) are straightforwardly modified to the present case: they remain the same for the lower face in Fig. 9 and use index substitution $k \to k+1$ for the upper face.

The coil of arbitrary orientation with the unit direction vector $\vec{n}$ is considered as a superposition of three coils directed along the *x*-, *y*-, and *z*-axes. The corresponding current densities are given by

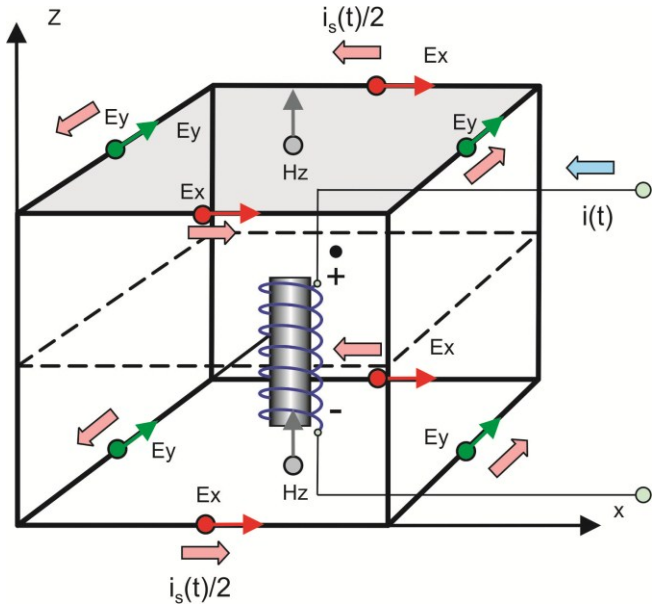

Fig. 9. Coil antenna model with the coil placed at the center node of the Yee cell.

$$J_{sX}(t)=\frac{1}{2}n_X\frac{AN}{\Delta^4}i(t),\quad J_{sY}(t)=\frac{1}{2}n_Y\frac{AN}{\Delta^4}i(t),\quad J_{sZ}(t)=\frac{1}{2}n_Z\frac{AN}{\Delta^4}i(t) \tag{20}$$

All the current densities should follow the *right-hand rule* with regard to all three Cartesian axes as shown in Fig. 9 for the z-axis.

The model described above was implemented in the code. It is advantage is the ability to describe the coil of arbitrary orientation, whilst keeping the same phase center. Its disadvantage is a "large" volume occupied by the coil model that extends to two unit cells in every direction. The above coil model may be treated as a *symmetric* point source model.

4. Mutual inductance between transmit and receive coils

Although not directly implemented in the code, the mutual inductance between transmit and receive coils as a function of frequency can be calculated after the FDTD run is finished. The result has the form

$$L_{m1}(\omega)=\frac{fft(E^m_{emf}(t))}{j\omega fft(i^1(t))}=-\mu_0 AN\frac{fft(H^m_{x,y,z}(t))}{fft(i^1(t))} \tag{21}$$

The self-inductance is found as described in subsection 1. Note that the current is to be given on half temporal grid – see Eqs. (17) whereas the emf voltage is found on the integer temporal grid – see Eq. (5b). Therefore, for example, one could interpolate the current for the integer temporal grid.

5. MATLAB implementation

The MATLAB implementation of the symmetric coil model (and of the related field probe) is given by the code that follows

```
%   FDTD MATLAB antenna/array solver
%   Copyright SNM/GN 2011
%   Electric-current coil antenna model (after E-field update)

%   setting up parameters
Js   = PortM(m)/d^4*(IG(m, kt)+IG(m, kt+1))/2;  %   volumetric current density
at n+1/2 - tested
i_e = PortIndX(m);   %   port location grid nodes
j_e = PortIndY(m);   %   port location grid nodes
k_e = PortIndZ(m);   %   port location grid nodes
Jx = d*Js/2*PortNX(m);
Jy = d*Js/2*PortNY(m);
Jz = d*Js/2*PortNZ(m);

%   coil/loop along the x-axis
%   Update equations (simple addition - right-hand rule exactly)
EzN(i_e, j_e, k_e)   = EzN(i_e, j_e, k_e)   + Ez2(i_e-1, j_e-1, k_e)*Jx;
EzN(i_e, j_e+1, k_e) = EzN(i_e, j_e+1, k_e) - Ez2(i_e-1, j_e, k_e)*Jx;
EyN(i_e, j_e, k_e)   = EyN(i_e, j_e, k_e)   - Ey2(i_e-1, j_e, k_e-1)*Jx;
EyN(i_e, j_e, k_e+1) = EyN(i_e, j_e, k_e+1) + Ey2(i_e-1, j_e, k_e)*Jx;

EzN(i_e+1, j_e, k_e)   = EzN(i_e+1, j_e, k_e)   + Ez2(i_e, j_e-1, k_e)*Jx;
EzN(i_e+1, j_e+1, k_e) = EzN(i_e+1, j_e+1, k_e) - Ez2(i_e, j_e, k_e)*Jx;
EyN(i_e+1, j_e, k_e)   = EyN(i_e+1, j_e, k_e)   - Ey2(i_e, j_e, k_e-1)*Jx;
EyN(i_e+1, j_e, k_e+1) = EyN(i_e+1, j_e, k_e+1) + Ey2(i_e, j_e, k_e)*Jx;
%   step n
AntEx        = 1/4*(ExP(i_e, j_e, k_e)+...
                    ExP(i_e, j_e+1, k_e)+...
                    ExP(i_e, j_e, k_e+1)+...
                    ExP(i_e, j_e+1, k_e+1));
%   E-fields for all ports -step n
AntHx  =    0.5*(HxN(i_e, j_e, k_e) + HxN(i_e+1, j_e, k_e));
%   H-fields for all ports -step n+1/2

%   coil/loop along the y-axis
%   Update equations (simple addition - right-hand rule exactly)
EzN(i_e, j_e, k_e)      = EzN(i_e, j_e, k_e)   - Ez2(i_e-1, j_e-1, k_e)*Jy;
EzN(i_e+1, j_e, k_e)    = EzN(i_e+1, j_e, k_e) + Ez2(i_e, j_e-1, k_e)*Jy;
ExN(i_e, j_e, k_e)      = ExN(i_e, j_e, k_e)   + Ex2(i_e, j_e-1, k_e-1)*Jy;
ExN(i_e, j_e, k_e+1)    = ExN(i_e, j_e, k_e+1) - Ex2(i_e, j_e-1, k_e)*Jy;
EzN(i_e, j_e+1, k_e)    = EzN(i_e, j_e+1, k_e)   - Ez2(i_e-1, j_e, k_e)*Jy;
EzN(i_e+1, j_e+1, k_e)  = EzN(i_e+1, j_e+1, k_e) + Ez2(i_e, j_e, k_e)*Jy;
ExN(i_e, j_e+1, k_e)    = ExN(i_e, j_e+1, k_e)   + Ex2(i_e, j_e, k_e-1)*Jy;
ExN(i_e, j_e+1, k_e+1)  = ExN(i_e, j_e+1, k_e+1) - Ex2(i_e, j_e, k_e)*Jy;
%   step n
AntEy         = 1/4*(EyP(i_e, j_e, k_e)+...
                    EyP(i_e+1, j_e, k_e)+...
                    EyP(i_e, j_e, k_e+1)+...
                    EyP(i_e+1, j_e, k_e+1));
%   E-fields for all ports -step n
AntHy   =     0.5*(HyN(i_e, j_e, k_e) + HyN(i_e, j_e+1, k_e));
%   H-fields for all ports -step n+1/2

%   coil/loop along the z-axis
%   Update equations (simple addition - right-hand rule exactly)
ExN(i_e, j_e, k_e)      = ExN(i_e, j_e, k_e)   - Ex2(i_e, j_e-1, k_e-1)*Jz;
```

```
ExN(i_e, j_e+1, k_e)     = ExN(i_e, j_e+1, k_e) + Ex2(i_e, j_e, k_e-1)*Jz;
EyN(i_e, j_e, k_e)       = EyN(i_e, j_e, k_e)   + Ey2(i_e-1, j_e, k_e-1)*Jz;
EyN(i_e+1, j_e, k_e)     = EyN(i_e+1, j_e, k_e) - Ey2(i_e, j_e, k_e-1)*Jz;
ExN(i_e, j_e, k_e+1)     = ExN(i_e, j_e, k_e+1)   - Ex2(i_e, j_e-1, k_e)*Jz;
ExN(i_e, j_e+1, k_e+1)   = ExN(i_e, j_e+1, k_e+1) + Ex2(i_e, j_e, k_e)*Jz;
EyN(i_e, j_e, k_e+1)     = EyN(i_e, j_e, k_e+1)   + Ey2(i_e-1, j_e, k_e)*Jz;
EyN(i_e+1, j_e, k_e+1)   = EyN(i_e+1, j_e, k_e+1) - Ey2(i_e, j_e, k_e)*Jz;

%   step n
AntEz          = 1/4*(EzP(i_e, j_e, k_e)+...
                      EzP(i_e+1, j_e, k_e)+...
                      EzP(i_e, j_e+1, k_e)+...
                      EzP(i_e+1, j_e+1, k_e));
%   E-fields for all ports -step n
AntHz    =     0.5*(HzN(i_e, j_e, k_e)+HzN(i_e, j_e, k_e+1));
%   H-fields for all ports -step n+1/2

%   co-polar components
AntE(m, kt) = PortNX(m)*AntEx + PortNY(m)*AntEy + PortNZ(m)*AntEz;
%   at step n - tested
TmpH(m, kt) = PortNX(m)*AntHx + PortNY(m)*AntHy + PortNZ(m)*AntHz;
%   at step n+1/2 - tested
AntH(m, kt) = (TmpH(m, kt) + TmpH(m, kt-1))/2;
%   at step n - tested
AntI(m, kt) = IG(m, kt);
%   at step n - tested
AntV(m, kt) = -mu0*PortM(m)*(TmpH(m, kt) - TmpH(m, kt-1))/dt;
%   antenna voltages for all ports at step n
```

The accuracy and limitations of the small symmetric-coil model have been quantified by many examples using the comparison with analytical solutions for point magnetic sources [3] reformulated in time domain.

6. References

[1]. G. S. Smith, *Loop Antennas*, In: J. L. Volakis, *Antenna Engineering Handbook*, fourth ed., McGraw Hill, 2007, pp. 5-3.

[2]. B. Z. Kaplan and U. Suissa, "Evaluation of inductance for various distributions of windings on straight ferromagnetic cores: an unusual approach, *" IEEE Trans. Magnetics*, vol. 38, no. 1, Jan. 2002, pp. 246-249.

[3]. C. A. Balanis, *Antenna Theory. Analysis and Design*, Third Ed., Wiley, New York, 2005.

[4]. R. Pontalti, J. Nadobny, P. Wust, A. Vaccari, and D. Sullivan, “Investigation of Static and Quasi-Static Fields Inherent to the Pulsed FDTD Method,” *IEEE Trans. Microwave Theory Techniques*, vol. 50, no 8, Aug. 2002, pp. 2022-2025.

impressed=effective

Section V. Model of an impressed electric field or voltage source (loop of magnetic current)

1. Concept of an impressed voltage (electric field) source

Considered two metal plates of area A separated by distance l in Fig. 10a with an applied voltage $\upsilon(t)$ between the plates. Assume that the corresponding electric field (directed down in Fig. 10a),

$$E_{in}(t) = \frac{\upsilon(t)}{l} \tag{1}$$

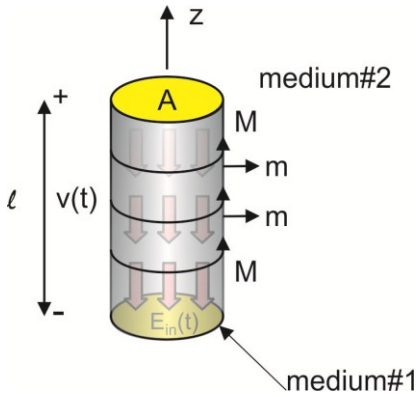

Fig. 10a. Impressed voltage (electric field source).

is uniform between the plates, which is true for small separation distances. Also assume that the electric field is zero otherwise (medium 2). The boundary condition for the electric field on the side boundary of the cylinder states that

$$\vec{M} = -\vec{m} \times (\vec{E}_2 - \vec{E}_{in}(t)) \tag{2}$$

where $\vec{M}$ is the resulting surface magnetic current density (V/m) on the side boundary, $\vec{m}$ is the outer normal. With reference to Fig. 1, $\vec{M}$ has only an angular component, i.e.

$$M_\varphi = E_{in}(t) = \frac{\upsilon(t)}{l} \tag{3a}$$

Thus, the impressed electric field source (or the voltage source) is equivalent to the loop of a surface magnetic current. The total magnetic current in the loop is lM_φ, the loop area is A. Therefore, the product $AlM_\varphi = A\upsilon(t)$ has the sense of a loop moment where A is the moment per one volt.

2. Modeling an impressed voltage source

The initial FDTD implementation is shown in Fig. 10b. The field source from Fig. 1 is placed at the node of the co-polar electric field as shown in Fig. 10b. Such a location is convenient, but it does not allow us to consider an arbitrary source orientation in general. We model the source with the closed loop of a magnetic current $i_{ms}(t)$ passing through the nodes for the magnetic field shown in the figure. This model is dual to the magnetic dipole. Since the loop moment should be preserved, it follows from Eq. (3a) that

$$i_{ms}(t) = \frac{A}{\Delta^2}\upsilon(t) \tag{3b}$$

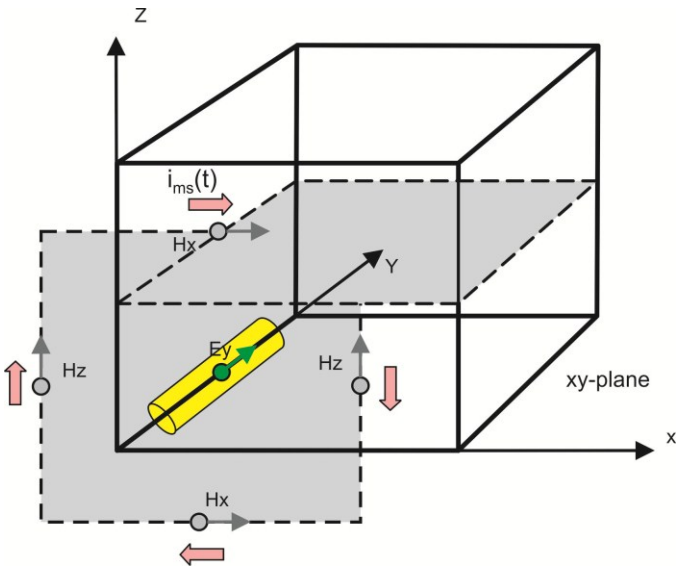

Fig.10b. TX voltage source and the surrounding FDTD grid.

Thus, the volumetric magnetic current density, $J_{ms}(t) = i_{ms}(t)/\Delta^2$, in Fig. 10b is specified. The update equations corresponding to Fig. 10b have the form

$$H_x^{n+1/2}(i,j,k) = H_{x1}H_x^{n-1/2}(i,j,k) + H_{x2}\times \\ \left(E_n^y(i,j,k+1) - E_n^y(i,j,k) + E_n^z(i,j,k) - E_n^z(i,j+1,k) - \Delta J_{ms}^n\right) \tag{4a}$$

$$H_x^{n+1/2}(i,j,k-1) = H_{x1} H_x^{n-1/2}(i,j,k-1) + H_{x2} \times \left(E_n^y(i,j,k) - E_n^y(i,j,k-1) + E_n^z(i,j,k-1) - E_n^z(i,j+1,k-1) + \Delta J_{ms}^n\right) \quad (4b)$$

$$H_z^{n+1/2}(i,j,k) = H_{z1} H_z^{n-1/2}(i,j,k) + H_{z2} \times \left(E_x^n(i,j+1,k) - E_x^n(i,j,k) + E_y^n(i,j,k) - E_y^n(i+1,j,k) + \Delta J_{ms}^n\right) \quad (4c)$$

$$H_z^{n+1/2}(i-1,j,k) = H_{z1} H_z^{n-1/2}(i-1,j,k) + H_{z2} \times \left(E_x^n(i-1,j+1,k) - E_x^n(i-1,j,k) + E_y^n(i-1,j,k) - E_y^n(i,j,k) - \Delta J_{ms}^n\right) \quad (4d)$$

An important observation is that it is very straightforward to implement Eqs. (4) in practice. Namely, only current excitation terms have to be added after the standard update equations for the magnetic field.

3. Modeling an impressed voltage source of arbitrary orientation

The magnetic current-loop model of Fig. 10b is straightforwardly modified for the case of arbitrary source orientation. The concept is shown in Fig. 11 that follows. The source antenna is now placed at the corner of the Yee cell. The source in Fig. 11 is replaced by *two* square loops of the grid-aligned magnetic current, which in sum possess the same moment. This means that the current density for each loop becomes the half of the original magnetic current density.

Update Eqs. (4) are straightforwardly modified to the present case: they remain the same for the upper face in Fig. 11 and employ the index substitution $j \to j-1$ for the lower face.

The source of arbitrary orientation with the unit direction vector $\vec{n}$ is considered as a superposition of three elementary sources directed along the *x*-, *y*-, and *z*-axes. The corresponding current densities are given by

$$J_{msX}(t) = \frac{1}{2} n_X i_{ms}(t), \quad J_{msY}(t) = \frac{1}{2} n_Y i_{ms}(t), \quad J_{msZ}(t) = \frac{1}{2} n_Z i_{ms}(t) \quad (5)$$

All the magnetic current densities should follow the *right-hand rule* with regard to all three Cartesian axes as shown in Fig. 11 for the y-axis.

The model described above was implemented in the code. It is advantage is the ability to describe the source of arbitrary orientation, whilst keeping the same phase center. Its disadvantage is a “large” volume occupied by the dipole model that extends to two unit cells in every direction.

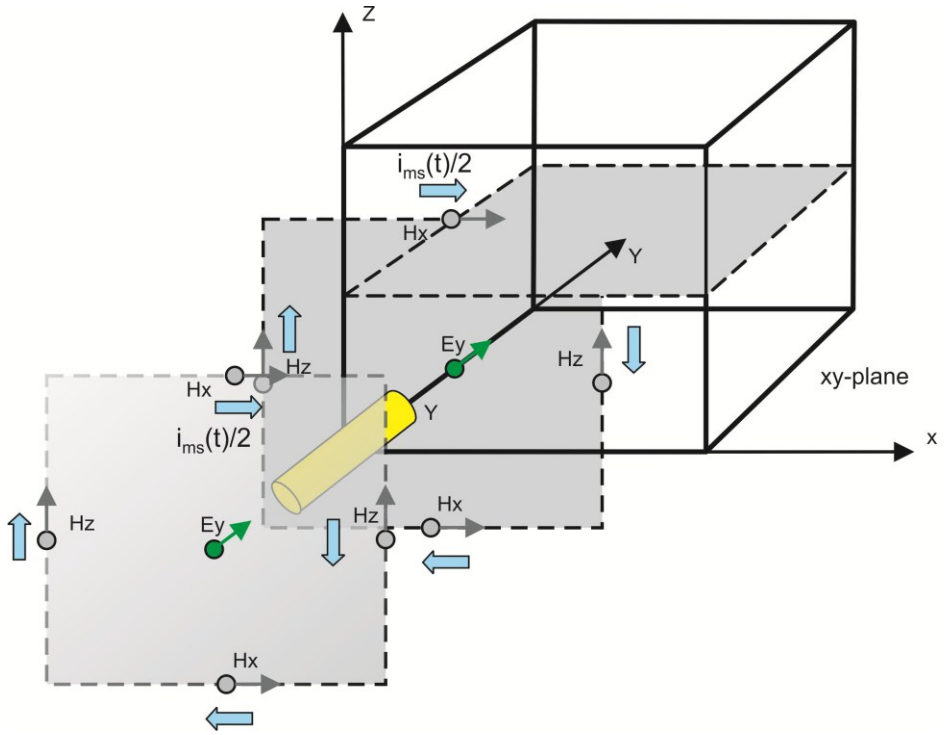

Fig. 11. Impressed source model with the dipole placed at the corner node of the Yee cell.

4. Relation between the magnetic current loop source and the electric dipole source

The displacement current (current in the capacitor) in Fig. 10a is directed down. Therefore, the counterpart of the magnetic current loop in Fig. 10a, with the magnetic current running following *the right-hand rule* with regard to the *positive* z-direction, should be an infinitesimally small electric dipole oriented toward the *negative* z-direction. If this dipole has a length l and a uniform line current $i_s(t) = I_{0s}\cos\omega t$, its radiation in the far field is described by ([1], Ch. 4, p. 159):

$$E_\theta = -j\frac{\eta k I_{0s} l}{4\pi r}\sin\theta\exp(-jkr)$$
$$H_\varphi = -j\frac{k I_{0s} l}{4\pi r}\sin\theta\exp(-jkr) \qquad (6)$$

On the other hand, the small magnetic current loop, whose right-hand rule axis is the z-axis, and which has a uniform magnetic current $i_{ms}(t) = I_{0ms}\cos\omega t$ and an area S, radiates in the far field in the following way:

$$E_\theta = \frac{k^2 I_{0ms} S}{4\pi r}\sin\theta\exp(-jkr)$$
$$H_\varphi = \frac{k^2 I_{0ms} S}{\eta 4\pi r}\sin\theta\exp(-jkr) \quad (7)$$

Comparing Eqs.(6) and (7) one has

$$k^2 I_{0ms} S = -j\eta k I_{0s} l \Rightarrow I_{0s} = jk\frac{S}{l\eta} I_{0m} \quad (8)$$

Eq. (8) can be transformed to the time-domain solution for an arbitrary pulse by operator substitution $jk \to c_0^{-1}\,\partial/\partial t$. This gives

$$i_s(t) = \varepsilon\frac{S}{l}\frac{\partial i_{ms}(t)}{\partial t} \Rightarrow i_{ms}(t) = \frac{l}{\varepsilon S}\int_0^t i_s(t')dt' \quad (9)$$

Further, the magnetic current $i_{ms}(t)$ is replaced by its current density uniformly distributed over every involved cell's cross-section:

$$J_{ms}(t) = \frac{i_{ms}(t)}{\Delta^2} = \frac{l}{\Delta^2\varepsilon S}\int_0^t i_s(t')dt' \quad (10)$$

Finally, since the loop area is the cell face, one has

$$J_{ms}(t) = \frac{l}{\Delta^4\varepsilon}\int_0^t i_s(t')dt' \quad (11)$$

The above expression has the units of V/m^2, indeed. The last step is to substitute into Eq. (11) the expression for $J_{ms}(t)$ that follows from Eq. (3b), that is

$$J_{ms}(t) = \frac{A\upsilon(t)}{\Delta^4} \quad (12)$$

The result becomes

$$i_s(t) = C\frac{d\upsilon}{dt}, \quad C = \frac{\varepsilon A}{l} \quad (13)$$

which is the familiar capacitor model introduced yet in the first figure to this section.

5. MATLAB implementation

The MATLAB implementation of the symmetric voltage source model is given by the code that follows

```
%   setting up parameters
Jms   = PortM(m)/d^4*VG(m, kt+1);
                      %   magnetic current/voltage at step n+1

i_e = PortIndX(m);    %   port location grid nodes
j_e = PortIndY(m);    %   port location grid nodes
k_e = PortIndZ(m);    %   port location grid nodes
Jx = d*Jms/2*PortNX(m);
Jy = d*Jms/2*PortNY(m);
Jz = d*Jms/2*PortNZ(m);

%   Port parameters
AntV(m, kt) = VG(m, kt);

%   impressed field along the x-axis
HyN(i_e, j_e, k_e)   = HyN(i_e, j_e, k_e)   + Hy2(i_e, j_e, k_e)*Jx;
HyN(i_e, j_e, k_e-1) = HyN(i_e, j_e, k_e-1) - Hy2(i_e, j_e, k_e-1)*Jx;
HzN(i_e, j_e, k_e)   = HzN(i_e, j_e, k_e)   - Hz2(i_e, j_e, k_e)*Jx;
HzN(i_e, j_e-1, k_e) = HzN(i_e, j_e-1, k_e) + Hz2(i_e, j_e-1, k_e)*Jx;

HyN(i_e-1, j_e, k_e)   = HyN(i_e-1, j_e, k_e)   + Hy2(i_e-1, j_e, k_e)*Jx;
HyN(i_e-1, j_e, k_e-1) = HyN(i_e-1, j_e, k_e-1) - Hy2(i_e-1, j_e, k_e-1)*Jx;
HzN(i_e-1, j_e, k_e)   = HzN(i_e-1, j_e, k_e)   - Hz2(i_e-1, j_e, k_e)*Jx;
HzN(i_e-1, j_e-1, k_e) = HzN(i_e-1, j_e-1, k_e) + Hz2(i_e-1, j_e-1, k_e)*Jx;

%   impressed field along the y-axis
HxN(i_e, j_e, k_e)   = HxN(i_e, j_e, k_e)   - Hx2(i_e, j_e, k_e)*Jy;
HxN(i_e, j_e, k_e-1) = HxN(i_e, j_e, k_e-1) + Hx2(i_e, j_e, k_e-1)*Jy;
HzN(i_e, j_e, k_e)   = HzN(i_e, j_e, k_e)   + Hz2(i_e, j_e, k_e)*Jy;
HzN(i_e-1, j_e, k_e) = HzN(i_e-1, j_e, k_e) - Hz2(i_e-1, j_e, k_e)*Jy;

HxN(i_e, j_e-1, k_e)   = HxN(i_e, j_e-1, k_e)   - Hx2(i_e, j_e-1, k_e)*Jy;
HxN(i_e, j_e-1, k_e-1) = HxN(i_e, j_e-1, k_e-1) + Hx2(i_e, j_e-1, k_e-1)*Jy;
HzN(i_e, j_e-1, k_e)   = HzN(i_e, j_e-1, k_e)   + Hz2(i_e, j_e-1, k_e)*Jy;
HzN(i_e-1, j_e-1, k_e) = HzN(i_e-1, j_e-1, k_e) - Hz2(i_e-1, j_e-1, k_e)*Jy;

%   impressed field along the z-axis
HxN(i_e, j_e, k_e)     = HxN(i_e, j_e, k_e)   + Hx2(i_e, j_e, k_e)*Jz;
HxN(i_e, j_e-1, k_e)   = HxN(i_e, j_e-1, k_e) - Hx2(i_e, j_e-1, k_e)*Jz;
HyN(i_e, j_e, k_e)     = HyN(i_e, j_e, k_e)   - Hy2(i_e, j_e, k_e)*Jz;
HyN(i_e-1, j_e, k_e)   = HyN(i_e-1, j_e, k_e) + Hy2(i_e-1, j_e, k_e)*Jz;

HxN(i_e, j_e, k_e-1)     = HxN(i_e, j_e, k_e-1)   + Hx2(i_e, j_e, k_e-1)*Jz;
HxN(i_e, j_e-1, k_e-1)   = HxN(i_e, j_e-1, k_e-1) - Hx2(i_e, j_e-1, k_e-1)*Jz;
HyN(i_e, j_e, k_e-1)     = HyN(i_e, j_e, k_e-1)   - Hy2(i_e, j_e, k_e-1)*Jz;
HyN(i_e-1, j_e, k_e-1)   = HyN(i_e-1, j_e, k_e-1) + Hy2(i_e-1, j_e, k_e-1)*Jz;
```

The accuracy and limitations of the small symmetric voltage-source model have been quantified by many examples using the comparison with the analytical solutions for point sources [1].

6. References

[1]. C. A. Balanis, *Antenna Theory. Analysis and Design*, Third Ed., Wiley, New York, 2005.

Section VI. Boundary conditions

1. Boundary conditions implemented in the code

A wide variety of Absorbing Boundary Conditions (ABCs) exist. A review of different ABCs is given in Ref.[1]; see also Ref.[2]. In this code, we will implement the first- and second-order ABCs due to Mur [3] augmented with Mei's superabsorption [4].

A simple yet reasonably accurate combination is that of the first-order Mur's ABCs and superabsorption. This combination does not need a special treatment for edges and corners. It is trivially extended to the case of an inhomogeneous medium and still has a sufficient numerical accuracy (second-order) as confirmed by a number of computational examples.

2. Mur's ABCs

Let's take a look at Fig. 12 that follows. First, if a source of excitation is located approximately in the center of the FDTD domain, and the size of this domain is large enough, the signal that hits the boundary is a combination of plane propagating waves.

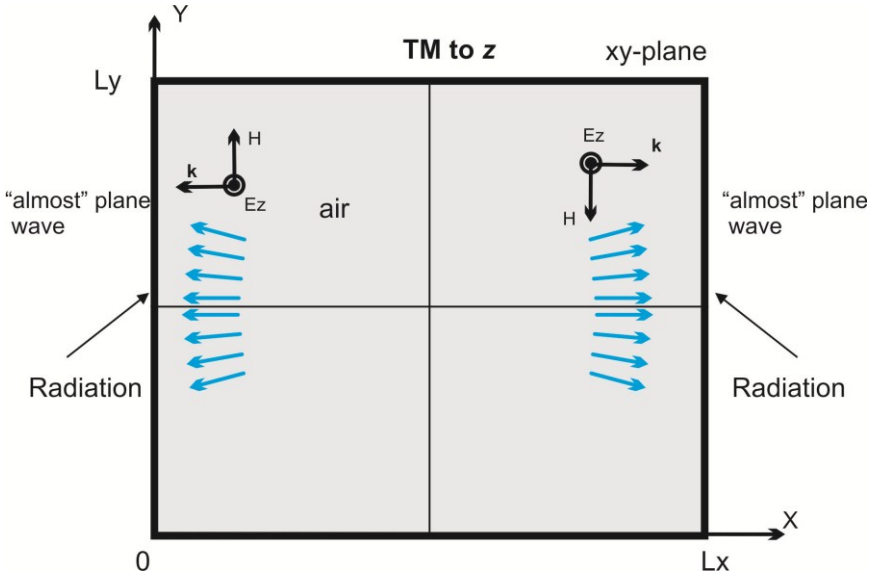

Fig. 12. An "almost" plane wave that is coming toward the boundaries needs to be absorbed.

Such a field is conventionally described in terms of the so-called *parabolic* approximation, which initially was developed for well-collimated weakly-diffracted optical beams - almost plane waves. Let us start with the wave equation for an arbitrary field quantity, W,

$$\frac{\partial^2 W}{\partial t^2} - c_0^2\left(\frac{\partial^2 W}{\partial x^2} + \frac{\partial^2 W}{\partial y^2} + \frac{\partial^2 W}{\partial z^2}\right) = 0 \tag{1}$$

One can obtain another form of this equation, to underscore the dominant propagation along the x-axis

$$\left(\frac{\partial}{\partial t} - c_0\frac{\partial}{\partial x}\right)\left(\frac{\partial}{\partial t} + c_0\frac{\partial}{\partial x}\right)W - c_0^2\left(\frac{\partial^2 W}{\partial y^2} + \frac{\partial^2 W}{\partial z^2}\right) = 0\,, \tag{2}$$

either in the positive or in the negative direction. We are interested in the boundary at x=0, i.e. in the negative direction of propagation. When the direction of propagation is *exactly* the negative x-axis and the wave is *exactly* plane, from Eq. (2) one obtains

$$\left(\frac{\partial}{\partial t} - c_0\frac{\partial}{\partial x}\right)W = 0 \tag{3}$$

While this observation is only approximately true, we could still replace one spatial derivative in the first term on the right-hand side of Eq. (2) by

$$\frac{\partial}{\partial t} \approx c_0\frac{\partial}{\partial x} \quad \Rightarrow \left(\frac{\partial}{\partial t} + c_0\frac{\partial}{\partial x}\right) \approx 2\frac{\partial}{\partial t} \tag{4}$$

This yields

$$\left(\frac{\partial}{\partial t} - c_0\frac{\partial}{\partial x}\right)\left(2\frac{\partial}{\partial t}\right)W - c_0^2\left(\frac{\partial^2 W}{\partial y^2} + \frac{\partial^2 W}{\partial z^2}\right) = 0 \tag{5}$$

or, which is the same,

$$\frac{\partial^2 W}{\partial t^2} - c_0\frac{\partial^2 W}{\partial t \partial x} - \frac{c_0^2}{2}\left(\frac{\partial^2 W}{\partial y^2} + \frac{\partial^2 W}{\partial z^2}\right) = 0 \tag{6}$$

Eq. (6) is the well-known *parabolic* approximation to the wave equation. It says that the electromagnetic signal propagates predominantly along the negative x-axis; it is also a subject to diffraction in the transversal plane (in the yz-plane). The parabolic equation is easier to solve than the wave equation itself, and it is straightforward to formulate the boundary conditions in terms of it. The first-order Mur's ABCs utilize Eq. (3); the second-order Mur's ABCs utilize Eq. (6).

First-order Mur's ABCs are given by Eq. (3) applied at all boundaries. In particular,

$$\frac{\partial E_z}{\partial t} - c_0 \frac{\partial E_z}{\partial x} = 0 \tag{7a}$$

$$\frac{\partial E_z}{\partial t} + c_0 \frac{\partial E_z}{\partial x} = 0 \tag{7b}$$

for the left and right boundary in Fig. 12, respectively. The results for the lower and upper boundaries are obtained by permutation (x→y). Despite this very simple nature, even those equations will do a decent job when implemented correctly.

Note: The first-order Mur's ABCs are given for the E-field only. The H-field is not involved. The reason becomes clear if we examine the field array:

```
% Allocate field matrices
Ex = zeros(Nx  , Ny+1, Nz+1);
Ey = zeros(Nx+1, Ny  , Nz+1);
Ez = zeros(Nx+1, Ny+1, Nz  );
Hx = zeros(Nx+1, Ny  , Nz  );
Hy = zeros(Nx  , Ny+1, Nz  );
Hz = zeros(Nx  , Ny  , Nz+1);
```

The component Hy, which might be a subject to the boundary conditions on the left/right boundary in Fig. 12 is simply not defined on those boundaries.

3. Implementation of the first-order ABCs

Let us proceed with the first-order Mur's ABCs Eqs. (7). The central point is how to implement them properly at the boundaries. We will use the central differences in both the space and the time increments, so that our result will have a local truncation error of the second order in all increments. One has

$$\frac{\partial E_z}{\partial t} - c_0 \frac{\partial E_z}{\partial x} = 0 \Rightarrow$$

$$\frac{1}{2}\left(\frac{E_{z1,j,k}^{n+1} - E_{z1,j,k}^{n}}{\Delta t} + \frac{E_{z2,j,k}^{n+1} - E_{z2,j,k}^{n}}{\Delta t} \right) - c_0 \frac{1}{2}\left(\frac{E_{z2,j,k}^{n+1} - E_{z1,j,k}^{n+1}}{\Delta} + \frac{E_{z2,j,k}^{n} - E_{z1,j,k}^{n}}{\Delta} \right) = 0 \tag{8a}$$

$$E_{z1,j,k}^{n+1} = E_{z2,j,k}^{n} + \frac{c_0 \Delta t - \Delta}{c_0 \Delta t + \Delta}\left(E_{z2,j,k}^{n+1} - E_{z1,j,k}^{n} \right), \quad j = 1 : N_y + 1, \quad k = 1 : N_z$$

for the left boundary. Eq. (8a) is valid for any node on the boundary, including the edges and the corners. When the inhomogeneous material properties are involved, the local speed of light $c = 1/\sqrt{\mu\varepsilon}$ is assumed to be constant close to the boundary in the direction perpendicular to the boundary, on both its sides. The tangential changes are allowed at

any node of the boundary; they are included into consideration exactly as in the main FDTD grid. For the right boundary in Fig. 12, one similarly has

$$\frac{\partial E_z}{\partial t} + c_0 \frac{\partial E_z}{\partial x} = 0 \Rightarrow$$

$$\frac{1}{2}\left(\frac{E_{z\,N_x+1,j,k}^{\,n+1} - E_{z\,N_x+1,j,k}^{\,n}}{\Delta t} + \frac{E_{z\,N_x,j,k}^{\,n+1} - E_{z\,N_x,j,k}^{\,n}}{\Delta t} \right) + c_0 \frac{1}{2}\left(\frac{E_{z\,N_x+1,j,k}^{\,n+1} - E_{z\,N_x,j,k}^{\,n+1}}{\Delta} + \frac{E_{z\,N_x+1,j,k}^{\,n} - E_{z\,N_x,j,k}^{\,n}}{\Delta} \right) = 0$$

$$E_{z\,N_x+1,j,k}^{\,n+1} = E_{z\,N_x,j,k}^{\,n} + \frac{c_0\Delta t - \Delta}{c_0\Delta t + \Delta}\left(E_{z\,N_x,j,k}^{\,n+1} - E_{z\,N_x+1,j,k}^{\,n} \right), \quad j = 1 : N_y + 1, \quad k = 1 : N_z \tag{8b}$$

The extensions to the lower and upper boundaries and to the 3D case are straightforward.

4. "Superabsorption" ABCs (*Mei and Fang* 1992)

The Mei-Fang "superabsorption" method [4] is not an ABC by itself, but rather a numerical procedure for the improvement of the local ABC's applied to the FDTD technique – see Ref. [5]. It embodies an error-canceling formulation according to which the same ABC is applied to both E anid H field components on and near the outer boundaries, depending on the polarization examined.

Namely, the calculation of the 2-D TM (TE) magnetic (electric) components, from their respective boundary ABC-derived electric (magnetic) ones, yields reflection errors which are strongly related to the errors in magnetic (electric) field components directly computed from the ABC. The opposite sign that these errors have in both of the above separate calculations is a point of crucial importance in the superabsorption procedure. Taking this fact into consideration and by properly combining the two different computations of the magnetic (electric) fields near the boundary, it is possible to cancel the reflection errors mutually while maintaining the correct values of the fields on the boundary [5].

Fig. 13 illustrates schematically the implementation of the method for the right boundary ($x = L$) of the computational domain in Fig. 12. For this boundary, we apply the first-order Mur's ABC given by Eq. (8b) not only to the Ez-field but also to the Hy-field in the vicinity to that boundary, i.e.

$$H_{y\,N_x,j,k}^{\,n+1/2(2)} = H_{y\,N_x,j,k}^{\,n-1/2} + \frac{c_0\Delta t - \Delta}{c_0\Delta t + \Delta}\left(H_{y\,N_x-1,j}^{\,n+1/2} - H_{y\,N_x,j,k}^{\,n-1/2} \right) \tag{9a}$$

Next, we compute the Hy-field by the regular finite-difference scheme to obtain

$$H_{y\,N_x,j,k}^{\,n+1/2(1)} \tag{9b}$$

Nx-1

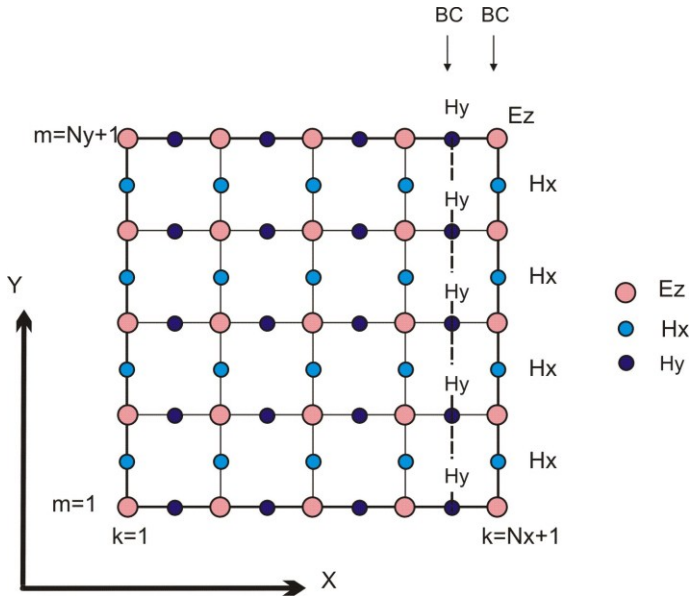

Fig. 13. Superabsorption ABCs on the right boundary.

After that, we form a weighted average of those two values and obtain the final updated magnetic field value a the last point by

$$H_{y\,N_x,j,k}^{\,n+1/2} = \frac{H_{y\,N_x,j,k}^{\,n+1/2(1)} + \rho H_{y\,N_x,j,k}^{\,n+1/2(2)}}{1+\rho} \tag{9c}$$

Here,

$$\rho = \frac{c_0 \Delta t}{\Delta} \tag{10}$$

It can be shown that this procedure significantly decreases the error of a local ABC, in particular, the first-order Mur's ABC. It is also very simply implemented and does not require any extra variables. When the inhomogeneous material properties are involved, the same scheme is followed as for the first-order Mur's ABCs.

5. MATLAB implementation in 3D

The MATLAB implementation of the ABCs is given by the code that follows (for a homogeneous medium)

First-order Mur's ABCs (after electric field update): **(for tangent fields on boundary)**

```
m1      = (c0*dt - d)/(c0*dt + d);
%   Left
EyN(1, :,:)    =  EyP(2,:,:)  + m1*(EyN(2,:,:) - EyP(1,:,:));      %  left - Ey;
EzN(1, :,:)    =  EzP(2,:,:)  + m1*(EzN(2,:,:) - EzP(1,:,:));      %  left - Ez;
```


P:Previous time-step
N:Now time-step

```
%   Right
EyN(Nx+1, :,:)=  EyP(Nx,:,:) + m1*(EyN(Nx, :,:) - EyP(Nx+1,:,:)); %   right - Ey;
EzN(Nx+1, :,:)=  EzP(Nx,:,:) + m1*(EzN(Nx, :,:) - EzP(Nx+1,:,:)); %   right - Ez;
%   Front
ExN(:, 1,:)    =  ExP(:,2,:)  + m1*(ExN(:,2,:) - ExP(:,1,:));      %   front - Ex;
EzN(:, 1,:)    =  EzP(:,2,:)  + m1*(EzN(:,2,:) - EzP(:,1,:));      %   front - Ez;
%   Rear
ExN(:, Ny+1,:)=  ExP(:,Ny,:) + m1*(ExN(:,Ny,:) - ExP(:,Ny+1,:));  %   rear - Ex;
EzN(:, Ny+1,:)=  EzP(:,Ny,:) + m1*(EzN(:,Ny,:) - EzP(:,Ny+1,:));  %   rear - Ey;
%   Bottom
ExN(:, :,1)    =  ExP(:, :,2)  + m1*(ExN(:,:,2) - ExP(:,:,1));     %   bottom - Ex;
EyN(:, :,1)    =  EyP(:, :,2)  + m1*(EyN(:,:,2) - EyP(:,:,1));     %   bottom - Ey;
%   Top
ExN(:, :, Nz+1)=  ExP(:,:,Nz) + m1*(ExN(:,:,Nz) - ExP(:,:,Nz+1)); %    top - Ex;
EyN(:, :, Nz+1)=  EyP(:,:,Nz) + m1*(EyN(:,:,Nz) - EyP(:,:,Nz+1)); %    top - Ex;
```

safe jeloi

safe poshti

Superabsorption ABCs (after magnetic field update):

```
coeff1  = (c0*dt - d)/(c0*dt + d);
rho     = c0*dt/d; RHO = 1 + rho;
%   Left
HyN(1,:,:) = (HyN(1,:,:) + rho*(HyP(2,:,:) + coeff1*(HyN(2,:,:) - HyP(1,:,:))))/RHO;
HzN(1,:,:) = (HzN(1,:,:) + rho*(HzP(2,:,:) + coeff1*(HzN(2,:,:) - HzP(1,:,:))))/RHO;
%  Right
HyN(Nx,:,:) = (HyN(Nx,:,:) + rho*(HyP(Nx-1,:,:) + coeff1*(HyN(Nx-1,:,:) -
HyP(Nx,:,:))))/RHO;
HzN(Nx,:,:) = (HzN(Nx,:,:) + rho*(HzP(Nx-1,:,:) + coeff1*(HzN(Nx-1,:,:) -
HzP(Nx,:,:))))/RHO;
%   Front
HxN(:,1,:) = (HxN(:,1,:) + rho*(HxP(:,2,:) + coeff1*(HxN(:,2,:) - HxP(:,1,:))))/RHO;
HzN(:,1,:) = (HzN(:,1,:) + rho*(HzP(:,2,:) + coeff1*(HzN(:,2,:) - HzP(:,1,:))))/RHO;
%   Rear
HxN(:,Ny,:) = (HxN(:,Ny,:) + rho*(HxP(:,Ny-1,:) + coeff1*(HxN(:,Ny-1,:) -
HxP(:,Ny,:))))/RHO;
HzN(:,Ny,:) = (HzN(:,Ny,:) + rho*(HzP(:,Ny-1,:) + coeff1*(HzN(:,Ny-1,:) -
HzP(:,Ny,:))))/RHO;
%   Bottom
HxN(:,:,1) = (HxN(:,:,1) + rho*(HxP(:,:,2) + coeff1*(HxN(:,:,2) - HxP(:,:,1))))/RHO;
HyN(:,:,1) = (HyN(:,:,1) + rho*(HyP(:,:,2) + coeff1*(HyN(:,:,2) - HyP(:,:,1))))/RHO;
%   Top
HxN(:,:,Nz) = (HxN(:,:,Nz) + rho*(HxP(:,:,Nz-1) + coeff1*(HxN(:,:,Nz-1) -
HxP(:,:,Nz))))/RHO;
HyN(:,:,Nz) = (HyN(:,:,Nz) + rho*(HyP(:,:,Nz-1) + coeff1*(HyN(:,:,Nz-1) -
HyP(:,:,Nz))))/RHO;
```

6. References

[1]. A. Taflove, *Computational Electrodynamics, The Finite Difference Time Domain Approach*, Third Ed., Artech House, Norwood, MA, 2005.

[2]. A. Bondeson, T. Rylander, and P. Ingelström, *Computational Electromagnetics*, Springer, New York, 2005, Series: Texts in Applied Mathematics , Vol. 51., pp. 58-86.

[3]. G. Mur, "Absorbing boundary conditions for the finite-difference approximation of the time-domain electromagnetic field equations," *IEEE Trans. Electromagn. Compat.*, vol. EMC-23, no. 4, pp. 377-382, Nov. 1981.

[4]. K. K. Mei and J. Fang, "Superabsorption – a method to improve absorbing boundary conditions," *IEEE Trans. Antennas and Propagation*, vol. 40, no. 9, Sep. 1992, pp. 1001- 1010.

[5]. N. V. Kantartzis and T. D. Tsiboukis, "A comparative study of the Berenger perfectly matched layer, the superabsorption technique, and several higher-order ABCs for the FDTD algorithm in two and three dimensional problems," *IEEE Trans. Magnetics*, vol. 33, no. 2, March 1997, pp. 1460-1463.